# Excitatory and Inhibitory Cable Properties Controls the Transient Amplification of Electrical Stimulation

**Maxim Piatine**

**Thesis submitted to the University of Ottawa in partial fulfillment of the requirements for the Master of Science in Physics**

**Department of Physics**
**Faculty of Science**
**University of Ottawa**

**Abstract**

Neuromodulation therapies such as deep brain stimulation have shown some clinical success in treating Parkinson's, epilepsy, essential tremor, and many other conditions. However, these devices primarily target the subcortex and treat a small subset of neurological disorders. To address these limitations, we investigate cortical stimulation as an alternative, focusing on the biophysical and network-level mechanisms that shape the brain's responses to electrical input.

This thesis investigates how excitatory and inhibitory cable properties influence the transient amplification resulting from electrical stimulation in the cortex. Cortical stimulation remains poorly understood, and debates persist about the biological processes involved in direct electrical stimulation. To better understand these responses, we developed a mathematical model grounded in the biophysical properties of neurons, combining axonal cable theory to emulate experimentally observed cortical phenomena.

We begin by analyzing recruitment through cable theory, and we derive a relationship between the intensity threshold and the axon diameter. Experimental studies (Micheva, Kristina D., et al., 2016) show that inhibitory axons in the cortex are larger in diameter compared to excitatory ones, resulting in a bias toward inhibitory recruitment. However, to promote excitatory recruitment, we assume that inhibitory axons, particularly those with larger diameters, are myelinated. Since myelinated axons require higher stimulus intensities to be activated, this assumption raises the activation threshold for inhibition, while favouring excitation. Therefore, the axonal cable properties in our model suggest that excitation is more readily recruited than inhibition.

Next, we develop the mean-field model, which begins with a network of intercommunicating excitatory and inhibitory neurons. We introduce two stimulation paradigms: the activation model, which focuses on the recruitment of antidromic axons and somas to initiate the input into our field model, and the depolarization model, which assumes direct electrical stimulation of neurons, leading them to depolarize in response to external extracellular voltage.

We find that both models elicit the same cortical responses from electrical stimulation. With fine-tuned parameters, both models exhibit transient amplification due to the excitatory-inhibitory imbalance in activation.

The cable properties of axons allow for the recruitment of excitatory and inhibitory neurons during electrical stimulation. The recruitment imbalance results in different network-level responses. In particular, our model demonstrates that these imbalances can lead to transient amplification, resulting in early excitatory activation followed by lagging inhibition that restores the network.

# Contents

# Acknowledgment

I want to take this opportunity to express my sincere and profound gratitude to my supervisor, Dr. Richard Naud, for his invaluable guidance and mentorship throughout the year. I am also sincerely thankful to Dr. Bela Joos for the opportunity to work on a biophysics project, the experience that greatly inspired me to continue in this field.

Most importantly, I want to thank my family for the unwavering support and encouragement throughout my education. A special thank you to Bill for staying up with me during the long nights of study and work. Your presence is deeply missed.

# List of Abbreviations & Symbols

List of abbreviations

| | |
|---|---|
| DBS | Deep brain stimulation |
| PD | Parkinson's disease |
| OCD | Obsessive-compulsive disorder |
| LFP | Local field potential |
| DES | Direct electrical stimulation |
| STN | Subthalamic nucleus |
| AP | Action potential |
| PSP | Postsynaptic potential |
| BCI | Brain computer interfaces |
| ICMS | Intracortical microstimulation |
| MFT | Mean-field theory |
| BG | Basal Ganglia |
| TMS | Transcranial magnetic stimulation |

List of Symbols

| | | | | | |
|---|---|---|---|---|---|
| $I_T$ | Intensity threshold | $I_\infty$ | Rheobase | $\Delta^*$ | Chronoxie |
| $V_{\text{stim}}$ | External stimulation | $V$ | Membrane potential | $C_m$ | Membrane capacitance |
| $R_m$ | Membrane resistance | $R_a$ | Axonal resistance | $\rho_a$ | axoplasm resistance |
| $\lambda$ | Electronic const. | $\tau_m$ | Membrane time const. | $v$ | Conduction velocity |
| $d$ | Diameter | $r$ | Radius | $w$ | Synaptic weight |
| $\nu$ | Mean firing rate | $\Theta$ | Heaviside function | $k$ | Direct electric effect |
| $\vartheta$ | Threshold potential | $\tilde{w}$ | Synaptic weight kernel | $T$ | Pulse duration |
| $V_{\text{rest}}$ | Resting potential | $q$ | Charge | $S$ | Spike train |
| $R$ | Electrode resistance | $\alpha$ | Offset parameter | $e$ | Excitatory |
| $i$ | Inhibitory | $I_{syn}$ | Synaptic current | $\epsilon$ | Postsynaptic potential |
| $\gamma$ | Gain parameter | $I_a$ | Axial current | $I_m$ | Membrane current |
| $I_c$ | Capacitative current | $t$ | Time | $\delta$ | Delta function |

# List of Figures



# List of Tables

# 1 Introduction

Neurological disorders are among the most disruptive and costly chronic conditions, affecting one in three people globally. That is close to three billion people affected by different conditions like epilepsy, dementia, Parkinson's, depression, and many more [1].

The current standard therapeutic approach to treat several of these neurological diseases is through direct electrical stimulation (DES) and pharmaceutical medications. While pharmaceutical interventions remain the first line of defense, over 200,000 patients have undergone necessary treatments worldwide, such as deep brain stimulation (DBS) [2]. DES involves applying low-amperage electrical stimulation to modulate neural circuits that have become dysfunctional or damaged due to these neurological disorders.

Despite clinical success, DBS primarily targets subcortical regions such as the thalamus. These approaches are highly invasive, limited to specific brain structures, and are only available to a small subset of patients. This thesis investigates cortical stimulation as a less invasive alternative to current neuromodulation techniques, such as DBS.

## 1.1 Neurophysiology & Neuronal Dynamics

Neurons are cells that send messages throughout the body, allowing us to perform a wide range of tasks, from breathing to talking, eating, walking, and thinking [39]. While there are many varieties of neurons, they all share three main components: the dendrites, which receive signals from other neurons (presynaptic neurons); the soma, which processes the input; and the axon, which transmits the signal from the soma towards the synapse, where it communicates with other neurons (postsynaptic neurons) [36]. In the synaptic cleft, the space between sending (presynaptic) and receiving (postsynaptic) neurons, communications can happen either chemically, through neurotransmitters binding to receptor proteins, or electrically, through direct ion flow along gap junctions [37, 38].

Neurons are characterized by their membrane potential, which is naturally negative, typically resting at -75 millivolts. This negative voltage is caused by the unequal distribution of ions compared to the outside, with the primary ions being sodium (Na+), potassium (K+), and chloride (Cl-) [40]. Over time, neurons undergo several phases, including depolarization, repolarization, and hyperpolarization [41]. Depolarization occurs when the membrane potential is less negative than its resting potential. This happens when the cell is positively stimulated by other cells through synaptic channels or externally stimulated by an electrode. Once depolarized to -55 millivolts, the neuron fires an action potential (AP), a short voltage pulse that propagates down the axon. Shortly after, the membrane potential will reach a peak voltage of around 35 millivolts. Then, the cell will repolarize, allowing potassium ions to exit the cell and restoring its negative potential. The cell then undergoes hyperpolarization, briefly becoming more negative than its resting potential before returning to its resting state [41, 42].

The Nernst equation describes a method for measuring the membrane potential of a cell by tracking the movement of ions across the cell membrane, as they move against their concentration gradients. The equation involves $R$ the gas constant, $T$ the temperature in kelvins, $F$ for Faraday's constant, $z$ the valance of the ion typically ranging from -1, 1, 2, and $[X]$ the ion concentration, the subscript indicates the concentration outside and inside the membrane [29]:

$$V_{eq} = V_{out} - V_{in} = \frac{RT}{zF} \ln\left(\frac{[X]_{out}}{[X]_{in}}\right) . \tag{1.1}$$

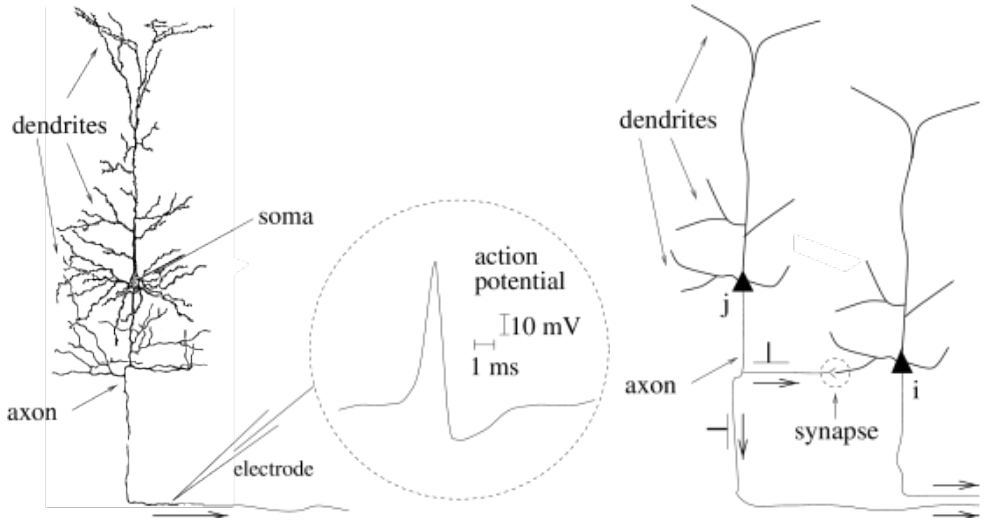


Figure 1: **Neuron Drawings**. **Left.** Single neuron in a drawing by Ramón y Cajal. The dendrites, soma, and axon are contrasted in the drawing. **Middle.** An action potential being recorded from the electrode targeting the axon. The action potential is a brief voltage pulse that is released from the neuron, where the neuron then undergoes phases of depolarization, repolarization, hyperpolarization, and a refractory period, after which the membrane returns to its resting state. **Right.** The signal transmission from presynaptic to postsynaptic neuron happens at the synapse (dashed circle). Figure reproduced with permission from *Cambridge University Press* [8].

Neurons are broadly classified into two functional types: excitatory and inhibitory. Excitatory neurons release neurotransmitters that help depolarize the postsynaptic neurons, while inhibitory neurons release GABAergic neurotransmitters, primarily causing polarization.

We can determine the membrane potential of a postsynaptic neuron based on the input received from the presynaptic neuron. Let $V_i$ be the membrane potential at time $t$. The sums of postsynaptic potentials (PSPs) $\epsilon_{ij}$ received from neuron $j$ to neuron $i$ at time $t^{(f)}$, and the resting membrane potential $V_{rest}$ [8] are related by:

$$V_i(t) = \sum_j \sum_f \epsilon_{ij} \left( t - t_j^{(f)} \right) + V_{rest} \ . \tag{1.2}$$

The equation describes the membrane potential of neuron $i$ that takes synaptic inputs from different neurons $j$, at times $t_j^{(f)}$. Once at threshold voltage ($\vartheta$), the neuron will fire an action potential (AP).

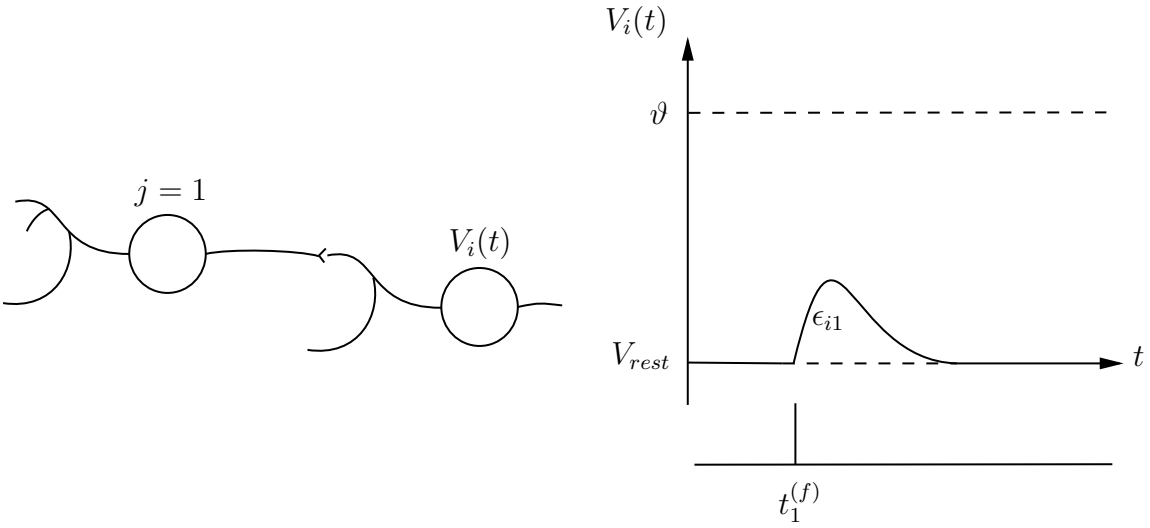


Figure 2: **Presynaptic synapse to postsynaptic potential**. A schema of the postsynaptic neuron $i$ receiving a spike from an excitatory presynaptic neuron $j$, resulting in an excitatory postsynaptic potential (EPSP). This EPSP can be measured with an electrode as the potential difference between its current state and resting state $V_i(t) - V_{rest}$. The time course of the EPSP, induced by the spike of neuron $j$, is described by $\epsilon_{i1}\left(t - t_1^{(f)}\right)$, which captures the stereotypical changes in the postsynaptic membrane potential following a presynaptic action potential at time $t_1^{(f)}$. When $V_i(t)$ reaches threshold $\vartheta$, an action potential is triggered. Reconstructed plot from [8].

We have seen how the membrane potential is modeled and how it is affected by ions or synaptic input. Additionally, external stimulation from electrodes and other electrically conducting devices can also modulate membrane potentials by delivering current to the surrounding tissue. While biological factors, such as ion dynamics and synaptic activity, control the generation of action potentials, there are instances where these dynamics are dysfunctional and require external intervention to induce charge into the tissue. This involves devices known as brain-computer interfaces (BCIs), which facilitate communication between neurons [43]. However, these devices can come with limitations, and will be explored in Section 1.3.

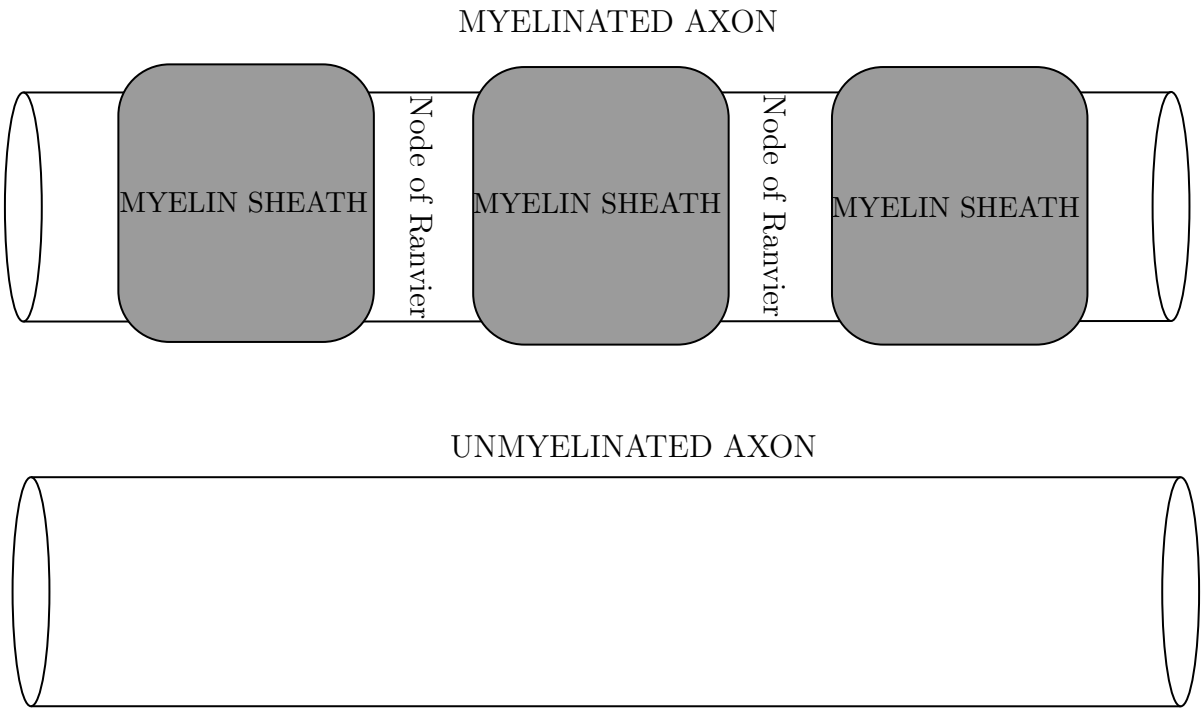


Figure 3: **Comparison between myelinated and unmyelinated axon**. The myelinated axon (top) is composed of insulating myelin sheath sections, that are spaced by the nodes of Ranvier. The unmyelinated axon (bottom) has no myelin sheath.

Because the axon is an extension of the cell body, it follows the functional classification of the neuron. Additionally, axons are classified based on whether they have an insulating sheath of myelin, resulting in unmyelinated and myelinated axons. Therefore, axons can come in a combination of excitatory-myelinated, excitatory-unmyelinated, inhibitory-myelinated, and inhibitory-unmyelinated.

Axons can be compared to electrical wires in a circuit, where action potentials formed by the soma propagate along cables connected to batteries. This presents an interesting perspective on the comparison between the circuitry in electrical engineering and the biological circuitry, comprising axons, somas, and dendrites. Therefore, axons, just like cables, act as conductors that propagate charge across their bodies to deliver it to a different part of the system.

The two significant differences between myelinated and unmyelinated axons are based on their physical properties. Myelinated axons come with an insulating fatty material that covers the membrane walls of the axons; however, this sheath is interrupted at regular intervals by the nodes of Ranvier, which form a slight separation between myelin and unmyelinated areas [30]. These structural differences enable the propagation of signals significantly faster than those in unmyelinated axons. For comparison, an unmyelinated

axon propagates an action potential at 0.5-2.0 m/s, while a myelinated axon propagates at 70-120 m/s [31]. This significant difference is due to the voltage-gated sodium channels that are present in the unmyelinated axons, which are distributed across the entire membrane, spanning the entire length of the axon, resulting in continuous depolarization. In contrast, myelinated axons only have the sodium channels at the nodes, allowing for saltatory conduction [31, 42].

Axonal dynamics strongly dependent on the diameter of the axon. It has been observed that the conduction velocity is proportional to the diameter $v \propto d^q$, where $q$ depends on whether the axon is myelinated ($q \approx 1$) or unmyelinated ($q \approx 0.5$) [61]. Thus, larger diameters contribute to higher conduction velocities [32]. This is due to the differences in axonal resistance ($R_a$) and membrane capacitance ($C_m$), which change with geometry [33].

Larger diameter axons are more easily recruited by low stimulation intensities, meaning that less current is required to depolarize the membrane. This is due to the axonal resistance ($R_a$) being smaller, as it is inversely proportional to diameter, and the membrane capacitance ($C_m$) being proportional to diameter, making the voltage potential dependent on the ratio of axonal resistance to membrane capacitance [17, 34].

However, the threshold current ($I_T$) is inversely related to the axon diameter at a rate that depends on the level of myelination on the axon. Since myelin acts as an insulating layer, it significantly alters the membrane capacitance ($C_m$) and the membrane resistance ($R_m$):

$$I_T \propto \frac{1}{d^q} \, . \tag{1.3}$$

where $q$ changes depending on myelinated and unmyelinated fibers.

## 1.2 Biophysics of Electrical Stimulation

Most DES devices use electrodes to deliver electrical current into the brain. Since electrodes are good electrical conductors, they inject charge into the tissue altering the environment of nearby neurons. This means that, for neurodegenerative disorders such as PD, the flow of charge increases or decreases the likelihood of cells firing depending on the target and context.

Extracellular potentials are often modeled under certain assumptions: an infinite, homogeneous, isotropic medium with constant resistivity $\rho$. Under these assumptions, the voltage at a distance $r$ from a monopolar spherical electrode delivering a current $I$ can be approximated as

$$V(r) = \frac{\rho I}{4\pi r} \ . \tag{1.4}$$

This approximation assumes a homogeneous tissue and that the surrounding tissue does not alter the field [17, 34]. The equation can change depending on the electrode configurations, such as the dipole configuration we see later in this thesis.

From extracellular fields and their approximation to stimulatingover neurons. There are two main ways of interaction. The first is the cell-field interaction, which is the direct localized extracellular electric field induced by an electrode. This localized field directly depolarizes or hyperpolarizes the neuronal membranes. The second mechanism is ephaptic coupling, where neurons that are excited by an external field can influence nearby cells, even in the absence of synaptic or physical connections [44]. The depolarization of one neuron may result in depolarization of the neighbouring cell.

A valid approximation for estimating the effect of the external stimulation on axons is with the activation function ($S$), where the electrical stimulation is a representation of the second derivative of the external potential in the direction of the axon ($x$) [34, 17]:

$$S = \frac{\partial^2 V_{ext}}{\partial x^2} \ . \tag{1.5}$$

Additionally, the strength-duration curve represents a relationship between the intensity and the duration of an electrical stimulus to evoke an action potential in a neuron or axon. As the intensity decreases, the stimulation duration decreases nonlinearly, following a hyperbolic decay $(1/T)$ (Figure 4). Meaning, if we take some intensity $I$ and apply it directly to an axon, it would take $T$ time to elicit activation from the axon, depending on whether the intensity is above rheobase $(I_\infty)$ [45, 46].

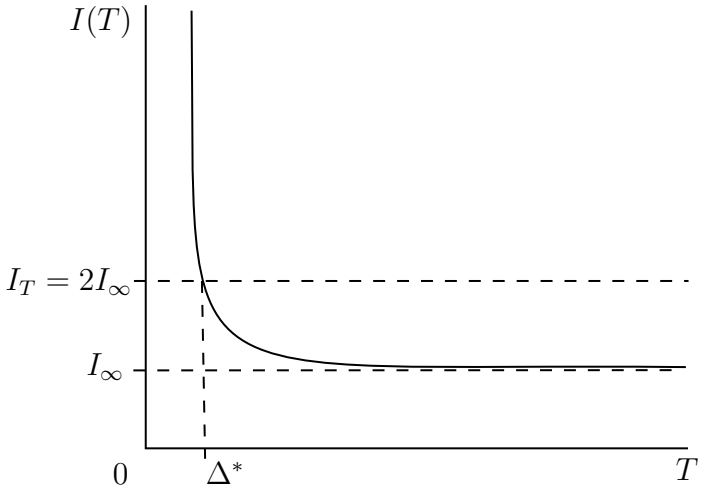


Figure 4: **Strength-intensity curve**. The relationship between stimulus intensity and duration required to activate an axon. $I_\infty$ is the rheobase, which is the minimum intensity to evoke an action potential. $I_T$ is the intensity threshold, which is double the rheobase. $\Delta^*$ is the chronaxie, which is the time needed to activate an axon at the intensity threshold $(I_T)$.

The rheobase $(I_\infty)$, is the lowest intensity strength we can apply to an axon at some time $T \to \infty$, to evoke an action potential. The chronaxie $(\Delta^*)$ is the time needed for the double of the rheobase, which is also known as the intensity threshold $(I_T)$.

$$I_T = 2 \cdot I_\infty \ . \tag{1.6}$$

Therefore, the strength-duration curve has the relationship:

$$I_T = I_\infty \left(1 + \frac{\Delta^*}{T}\right) \ . \tag{1.7}$$

By examining the relationship between intensity threshold and axon diameter, we can formulate a definition of the strength-duration curve that incorporates the diameter variable [34, 17].

Intracranial stimulation devices utilize the local field potential (LFP), the summed population of activity across thousands of cells and synapses, to deliver an appropriate amount of stimulation. Since the 1950s, extensive research has been conducted on network connectivity using single-pulse electrical stimulation to induce corticocortical evoked potentials [47]. This work provided valuable insights into the different responses in various brain regions resulting from induced cortical stimulation [48]. Beyond mapping, trains of stimulation pulses are closely associated with therapeutic applications [49]. At high frequencies ($>$ 100 Hz), stimulation improves memory, alleviates OCD symptoms, and reduces motor symptoms such as rigidity associated with Parkinson's disease. At lower frequencies ($\sim$10 Hz), the stimulation is therapeutic in epilepsy [50, 51, 52].

## 1.3 Limitations of Current Stimulation Paradigms

DES uses low-amperage electrode stimulation to evoke action potentials in a group of neurons, depending on the neurological disorder. Neurological disorders lack particular circuitry to allow for normal operations; the current solutions to help with regaining these operations are through medications or DES. In the case of Parkinson's disease, according to the National Institute of Health, over 81% of patients with PD were prescribed medication. In contrast, 76% of PD patients found the medication to wear off over time [3, 4]. The alternative is deep brain stimulation (DBS). Since the 1980s, an estimated 160,000 people have undergone a procedure to implant a deep brain stimulation device. This medical device involves electrical stimulation from electrodes placed in the subcortical part of the brain, specifically the basal ganglia, which is responsible for the body's voluntary movements, decision-making, reward, and addiction [5, 6].

Although deep brain stimulation (DBS) devices are used to treat various neurological disorders, the operation of the device differs depending on the disorder. For instance, in Parkinson's disease, therapeutic devices target the circuits in the basal ganglia to compensate for reduced dopamine. While in epilepsy, DBS devices may target inhibitory neurons to suppress seizures.

Nonetheless, a minimal number of PD patients qualify for these devices. A study found that only 1.6% of patients met the criteria for subthalamic nucleus DBS, while more flexible criteria expanded eligibility to 4.5% [53]. Unfortunately, these criteria are due to a variety of reasons and not necessarily biological qualifications. For instance, a surgical operation and implantation can cost over 40,000$ [54]. Moreover, DBS device patients typically have a life expectancy of 10 years, with a 51% chance of survival rate post DBS implants [7].

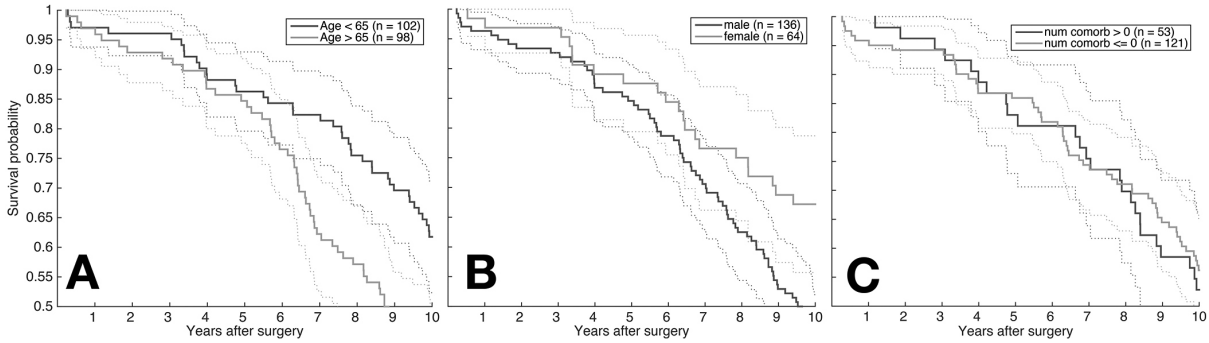


Figure 5: **Survival Rate Post DBS**. The Kaplan-Meier survival curve analysis shown for **A** ages over and under 65, **B** for male and female patients, and **C** the number of comorbidities, where $> 0$ is the patients who have at least one comorbidity. The analysis is based on the probability of survival post DBS surgery, resulting in 50% chance of survival post 10 years post implantation. Figure reproduced with permission from the *Journal of Neurosurgery*. [7].

From the figure, it is evident that there is a decline in survival probability, as indicated by the Kaplan-Meier survival curve analysis. We know that DBS devices are highly invasive systems that have an electrode probe that is implanted to stimulate the Subthalamic Nucleus (STN). The explanation for this is that DBS systems do not work efficiently over time for PD patients. Infections, strokes, and intracranial bleeding can all be factors of surgical complications that increase the risk of mortality [55].

While DBS is a powerful framework that has been built to solve neurological disorders in deep structures, such as the STN, diseases like depression, Alzheimer's, or stroke may involve distributed cortical networks that DBS cannot easily reach, which means that DBS' limitations are the ability to target motor symptoms, invasiveness, and potential side effects, not a one-size-fits-all solution.

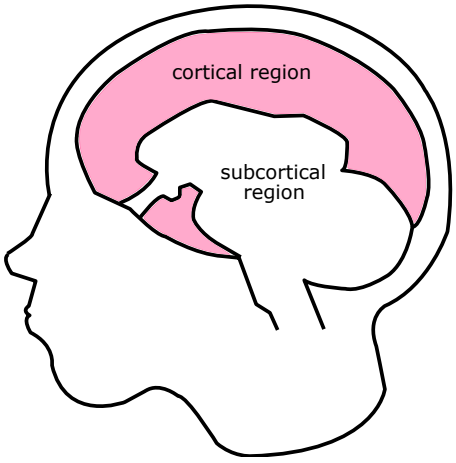


Figure 6: **Cortex & Subcortex**. A depiction of the focused brain regions for the subcortical and cortical regions. The subcortex is somewhat better understood by neuroscientists; however, the cortex is less well understood due to the high variability in the interconnections between excitatory and inhibitory connections, as well as recurrent networks.

## 1.4 Cortical Stimulation

Cortical stimulation involves applying electrodes to the surface of the cortex, the outer layer of the brain, and delivering electrical currents. It can be a powerful tool for mapping neural circuits and aiding in the recovery of impaired sensory functions, such as vision, hearing, and touch [13].

Cortical stimulation differs from the currently existing neuromodulation tools, such as deep brain stimulation (DBS) or transcranial magnetic stimulation (TMS). DBS devices are implanted in the subcortex, located underneath the cortex layer, and deliver electrical pulses to regions such as the Basal Ganglia (BG). TMS devices are non-invasive and deliver stimulation through the scalp.

Although cortical stimulation targets specific areas of the brain to activate specific brain networks, the mechanisms underlying cortical stimulation are yet to be fully understood. Responses to direct electrical stimulation can vary across different cortical regions.

In 1968, Stoney and colleagues conducted an experiment designed to determine the extent of intracortical stimulating currents by examining thresholds for direct excitation of single pyramidal tract (PT) cells by placing electrodes near the cell [12]. After finding the PT cell from backpropagating AP from axons, the voltage in the medium could be represented by equation 1.4. Then Stoney and colleagues proposed that the relationship between threshold current and distance from the electrode for each cell can be expressed by [12]:

$$I = kr^2 \ . \tag{1.8}$$

where $I$ is the stimulating current ($\mu A$), $r$ is the distance between neuron and stimulating electrode ($\mu m$), and $k$ is the current and distance constant ($\mu A/\mu m^2$) [13]. These findings suggest that the radius of activated tissue around the electrode tip increases with the square root of the current intensity.

Histed and colleagues, on the other hand, used two-photon imaging of calcium imaging to understand the quantity of activated neurons based on the intracortical microstimulation (ICMS) intensity in the cortex. In the experiments, the electrode was shifted at small distances to observe the pattern of activation, with some experiments conducted using synaptic blockers. They found that increasing stimulation intensity recruited more neurons, but the radial extent of somatic activation remained unchanged. This result shows a contrast with Stoney et al., which predicted that higher intensities would activate more neurons over a wider spatial range [13, 14].

These perspectives highlight the complexity of cortical stimulation, thereby providing a rationale for developing a biophysical model of cortical stimulation.

## 1.5 Complexity of Cortical Networks & Amplifications

The cortex is composed of densely interconnected and recurrent networks, meaning that excitatory-to-excitatory, inhibitory-to-inhibitory, excitatory-to-inhibitory, and inhibitory-to-excitatory synaptic connections occur while excitation dominates the majority of synapses in the cortex, inhibition corresponds to approximately one-third of the synapses; however, despite the asymmetry, inhibition maintains a balance with excitation [24]. Therefore, the E/I balance in synaptic inputs differs from that of the subcortical regions, where most of the signal is feedforward rather than recurrent.

The balance between excitatory and inhibitory (E/I) refers to the synaptic inputs between excitatory and inhibitory during neural events or stimulation. Our brain attempts to maintain a balance in synaptic inputs that neurons or groups of neurons receive, as excitation and inhibition tend to balance their strength with one another [35]. The balance between excitation and inhibition can give rise to three different network responses:

1) non-amplification case, where the excitation and inhibition strengths are matched or dominated by inhibition, causing temporary excitation followed by immediate dissipation in activity ($E \lesssim I$);

2) the amplification case, where the excitation remains unchecked and is never inhibited, can occur in neurodegenerative diseases such as epilepsy ($E \gg I$) [56];

3) Lastly, the transient amplification case, where excitation temporarily leads while inhibition lags ($E > I$), produces a short-lived amplification before inhibition restores the balance. This outcome is theoretically linked to the non-normal amplification, where transient amplifications arises due to particular activity in the network [57]. The transient amplification has been proposed to account for the variable spontaneous activity patterns observed in the visual cortex in the absence of stimuli [58]. Experimental evidence for transient amplification from electrical stimulation has been observed in slice (unpublished data from Sydney S. Cash).

These different network responses arise from the complicated recurrent dynamics of cortical circuits [35]. A small imbalance in E/I ratios results in different network states. This thesis will explore these network responses through the lens of direct electrical stimulation using axonal activation recruitment to depolarize neurons.

## 1.6 Main Research Question

This thesis investigates the biophysical and network-level mechanisms underlying the transient amplification response to direct electrical stimulation (DES). We specifically ask ourselves: *How do excitatory and inhibitory cable properties control the transient amplification of cortical activity following electrical stimulation?* This question arises from the limitations of the currently existing neuromodulating devices, such as DBS, that do not target cortical circuits. In the following chapters, we will derive analytical solutions to the axonal cable theory using the network-level field model. We then explore how subtle differences in axon diameter, myelination, and excitatory-inhibitory imbalances can bias recruitment and shape network responses.

# 2 Cable Properties

In the preceding chapter, we mentioned the different morphologies of neurons and how they have dendrites, somas, and axons that play a role in propagating APs. In this chapter, we focus on the axon and its biophysical properties to understand how the variation in axonal geometry can lead to an imbalanced activation under electrical stimulation.

When we refer to cables and their dynamics, we refer to axons. Just as in any circuit operation, in neuroscience, axons are considered to function similarly to cables in circuits. While their dynamics might differ from the real world, axons and cables behave in a similar manner from propagating current.

We present the general derivation of the cable equation, which will be used as an introduction to present general variables in the upcoming derivations. Additionally, using the knowledge of the strength-intensity curve and the relationship between chronaxie $\Delta^*$ and conduction velocity $v$, we derive a new distribution for the intensity threshold based on axon diameters.

The purpose is to understand the intensity thresholds required to stimulate axons depending on the size of their diameter. With this information, we will be able to evaluate the necessary bias needed to evoke transient amplification from the axons based on the imbalance of the activation.

## 2.1 Cable Theory

To derive the relationship between the intensity needed to stimulate an axon and its diameter, we will start by deriving the cable equation to model the potential along passive axons. We break down the problem by mapping out the axon as a cylinder with segments of membrane capacitances $C_m$, membrane resistances $R_m$, and axonal resistances $R_a$ on the inside parallel to the membrane walls (Figure 7).

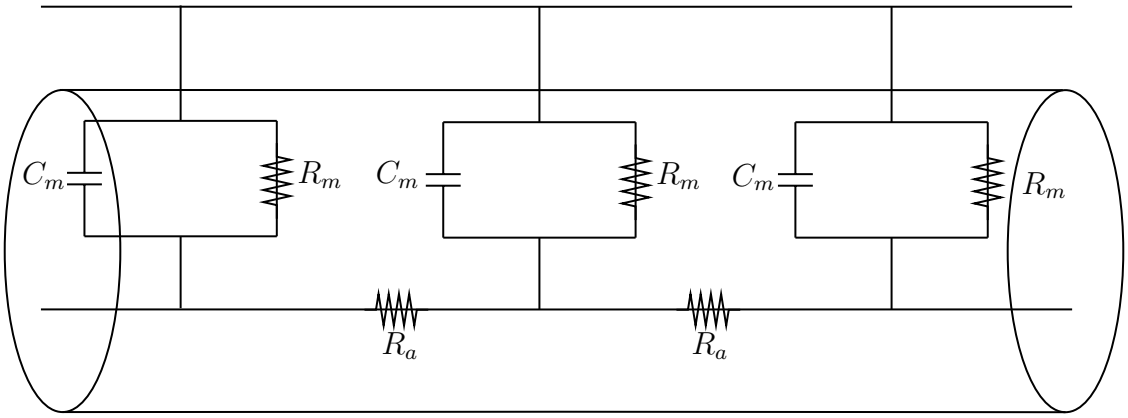


Figure 7: **Cable theory circuit for neurites**. The one-dimensional representation of a cylindrical cable with axonal resistance $R_a$, membrane resistance $R_m$, and membrane capacitance $C_m$ separating the outside and the inside of the membrane.

In the cable equation, the $R_a$ comes from the axoplasm $\rho_a$ ($\Omega m$) and determines the charge that passes depending on the diameter of the axon. If the diameter is larger, it will have less resistivity than a thinner axon, meaning the axonal resistance is dependent on the cross-sectional area $\pi r^2$, where $r$ is the radius. Thus, we measure $R_a$ to be in ohms per meter ($\Omega/m$):

$$R_a = \frac{\rho_a}{\pi r^2} \quad . \tag{2.1}$$

The $R_m$ is dependent on the number of ions that leak through the membrane, which is dependent on the circumference of the axon $2\pi r$ and the resistance for one unit area of membrane $r_m$ measured in ohms meters ($\Omega m$).

$$R_m = \frac{r_m}{2\pi r} \quad . \tag{2.2}$$

Lastly, $C_m$ depends on the amount of charge that moves through the membrane, which is dependent on the circumference, as well as $2\pi r$, and the capacitance of one unit area of the membrane, $c_m$, measured in farads per meter $(F/m)$.

$$C_m = c_m 2\pi r \quad . \tag{2.3}$$

Now, if we take a point $\Delta x$ to isolate a single circuit from the infinite cable, we would get an RC circuit. Let us seal the membrane $C_m = 0$ and $R_m \to \infty$ so no current flows across the membrane [16]. We can represent the axial current and the intracellular voltage with Ohm's law:

$$\begin{aligned} \Delta V &= -I_a R_a \Delta x \\ \frac{\Delta V}{\Delta x} &= -I_a R_a \\ \frac{\partial V}{\partial x} &= -I_a R_a \\ \frac{1}{R_a}\frac{\partial V}{\partial x} &= -I_a \quad . \end{aligned} \tag{2.4}$$

Considering that there is current escaping through the membrane $I_m$, and there is a change of current throughout the axoplasm $I_a$, we can use Kirchoff's law to represent the membrane current as:

$$\frac{\partial I_a}{\partial x} = -I_m = -\left(\frac{V}{R_m} + C_m \frac{\partial V}{\partial t}\right) \quad . \tag{2.5}$$

where $I_m$ is the current from the capacitance $I_c$ and resistance $I_r$ in the membrane circuit.

Inputting Equation 2.4 into 2.5, we obtain the partial differential equation from the cable theory [15, 16].

$$\tau_m \frac{\partial V}{\partial t} = -V + \lambda^2 \frac{\partial^2 V}{\partial x^2} \quad . \tag{2.6}$$

where $\tau_m$ is the membrane time constant in seconds and $\lambda$ is the electronic constant in meters:

$$\tau_m = R_m C_m \qquad\qquad \lambda = \sqrt{\frac{R_m}{R_a}} \quad . \tag{2.7}$$

The cable theory Equation 2.6 can be used to estimate the membrane potential in axons, as well as dendrites. With the addition to the voltage triggered by the electrical impulse stimulation $V_{\text{stim}}\delta(t)$:

$$\tau \frac{\partial V}{\partial t} = -V + \lambda^2 \frac{\partial^2 V}{\partial x^2} + V_{\text{stim}}(x)\delta(t) \quad . \tag{2.8}$$

where the external stimulation resembles the activation function seen in Section 1.2. To derive the strength-duration curve from equation 2.8, scientists have used the Hodgkin-Huxley model [34, 17].

## 2.2 Axon Intensity Threshold Distribution

We have uncovered the intensity threshold equation, also known as the strength-duration curve (Equation 1.7) in the Introduction. A paper by Nowak and Bullier on axons, which found the relation between the logarithmic chronaxie and the log conduction velocity of an action potential propagating through an axon, is $\log(\Delta^*) = -0.71\log(v) + 2.212$ [9].

$$\Delta^* = \frac{e^{2.212}}{v^{0.71}} \quad . \tag{2.9}$$

Additionally, the conduction velocity of an unmyelinated axon is proportional to the electric constant $\lambda$ over the membrane time constant $\tau_m$:

$$v \propto \frac{\lambda}{\tau_m} = \frac{\sqrt{\frac{d \cdot r_m}{4\rho_a}}}{\frac{r_m c_m}{(\pi d)^2}} \propto \sqrt{d} \quad . \tag{2.10}$$

$$\Delta^* = \frac{e^{2.212}}{v^{0.71}} \propto \frac{e^{2.212}}{d^{0.355}} \quad . \tag{2.11}$$

Now, plugging 2.11 into 1.7:

$$I_T \propto I_\infty \left(1 + \frac{e^{2.212}}{T d^{0.355}}\right) \quad . \tag{2.12}$$

From literature, the chronaxie is proportional to the inverse of the conduction velocity. We have now effectively found a way to rearrange the strength-duration curve with respect to diameter, which corresponds well with experimental observations where conduction velocity is inversely proportional to chronaxie and directly proportional to axon diameter [18, 19].

So now, there is a relationship between the intensity threshold and the diameter of an axon. To determine the distribution of axon diameters, we have observed that cortical region axons that are GABAergic are thicker on average than non-GABA axons.

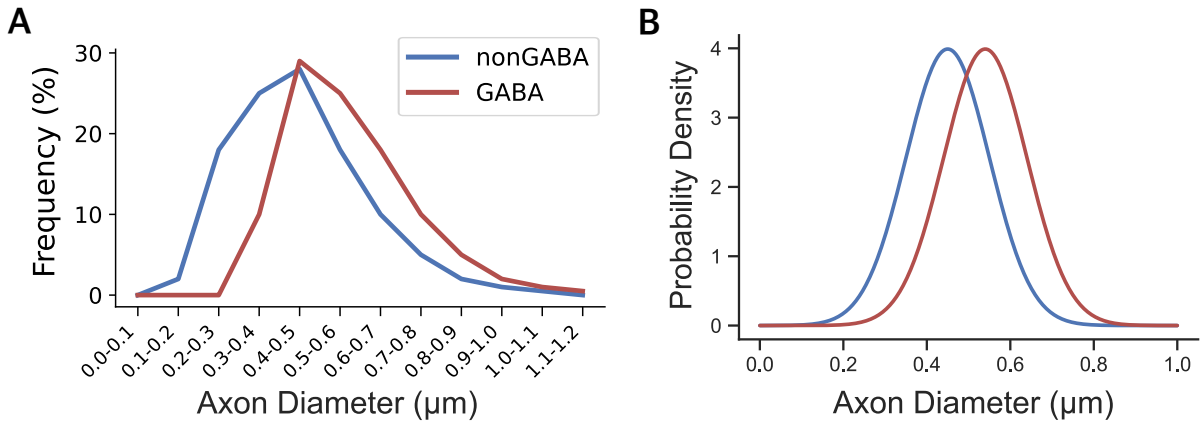


Figure 8: GABA and nonGABAergic axon diameter distribution. **a** Experimental frequency distribution plot of thickness of 163 GABA and 238 non-GABA axons [10]. **b** Theoretical axon diameter probability distribution function based on the experimental data in **a**. The blue line corresponds to an excitatory, and the red line corresponds to the inhibitory axon distribution.

Based on the Figure 8**A**, the derived distribution in 8**B**, results in an average inhibitory axon around $0.54 \pm 0.1\mu m$ and excitatory average of $0.45 \pm 0.1\mu m$.

The purpose of the derivation of this distribution is to explore the minimum intensity needed to stimulate an axon based on its diameter. Post DES, there is a spatial intensity fall-off, and we would like to know how many axons are recruited depending on the intensity. Therefore, we begin with the known diameter distribution (Figure 8**b**), which resembles a normal distribution. Once we derive the new distribution, we will be able to determine the probability of excitatory and inhibitory axons being recruited.

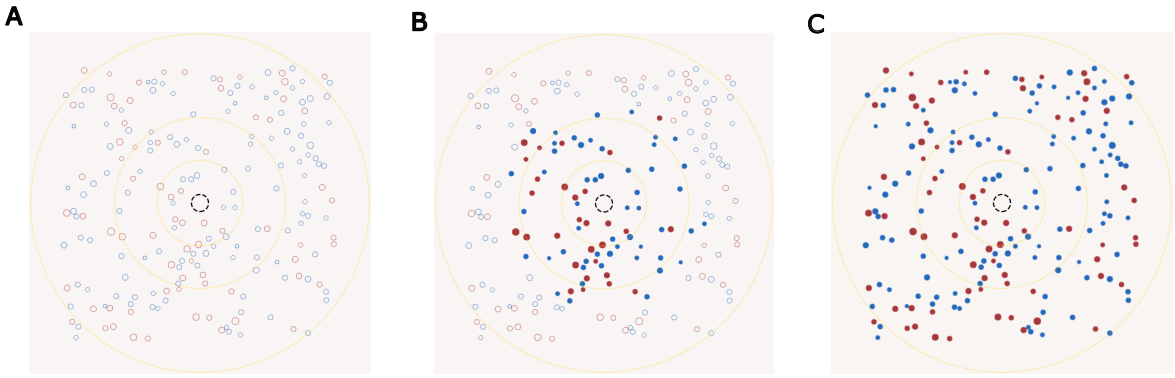


Figure 9: **Axonal recruitment from intensity progression**. A simulated axonal activation based on intensity strengths, where the red and blue circles are inhibitory and excitatory axons, respectively. The dashed black circle represents the origin of the electrode, while the three faint yellow circles have radii of 25, 50, and 100 microns. **a** No activation from a $10\mu A$ stimulus. **b** Partial recruitment from a $250\mu A$ stimulus. **c** The majority of axons are recruited with a $500\mu A$ stimulus.

The probability density function for diameter:

$$\mathbb{P}(d|\mu_d, \sigma_d) = \frac{1}{\sigma_d\sqrt{2\pi}} e^{-\frac{(d-\mu_d)^2}{2\sigma_d^2}} \quad . \tag{2.13}$$

Since there is an interest to determine the intensity threshold of our axons, there will be a change of variable.

$$\mathbb{P}(I_T) = \mathbb{P}(d) \left| \frac{\partial d}{\partial I_T} \right| \quad . \tag{2.14}$$

the partial derivative resulting in:

$$\left| \frac{\partial d}{\partial I_T} \right| = \frac{200}{71} \left( \frac{e^{2.212}}{T} \right)^{200/71} \frac{1}{I_\infty \left( \frac{I_T}{I_\infty} - 1 \right)^{271/71}} \quad . \tag{2.15}$$

After moving around the definition of intensity threshold to be a function of diameter with respect to threshold 2.12.

$$d(I_T) = \left[ \frac{I_\infty e^{2.212}}{T(I_T - I_\infty)} \right]^{\frac{200}{71}} \quad . \tag{2.16}$$

We plug $d(I_T)$ into the probability distribution function 2.13:

$$\mathbb{P}\left(d(I_T)\right) = \frac{1}{\sigma_d\sqrt{2\pi}} \exp\left\{ -\frac{\left(d(I_T) - \mu_d\right)^2}{2\sigma_d^2} \right\} \quad . \tag{2.17}$$

The result is a new non-normal distribution function that gives us information on the ratio of activated axons based on the intensity.

$$\mathbb{P}(I_T) = \frac{200 d(I_T)}{71\sigma_d\sqrt{2\pi}} \exp\left\{ -\frac{\left(d(I_T) - \mu_d\right)^2}{2\sigma_d^2} \right\} \quad . \tag{2.18}$$

# 3 Network Response to Electrical Stimulation

In the field model, we need to account for the behaviour of stimulation post DES. We know two main groups of neurons behave differently; the excitatory neurons positively affect the postsynaptic neurons via APs, while the inhibitory neurons have the opposite effect, as does their recurrent behaviour in the cortex. We've previously introduced the shape of monopolar and dipolar stimulation and the behaviour of the potential as a function of distance. Additionally, there are the controversies surrounding ICMS: In Stoney's worldview, as intensity grows, spatial expansion grows parabolically; while Histed's perspective is that the increase in intensity does not necessarily result in spatial expansion, but rather a more sparse activation within the volume. Lastly, three different cortical activity patterns result from DES.

In this chapter, we will derive the field model that will be used in Stoney's and Histed's worldviews, which we will later name the "Depolarization" and "Activation" models, respectively. To start, we will introduce the Leaky-Integrate and Fire (LIF) general model and its derivation, followed by the field model derivation, and we will introduce the parameters that affect the transient amplification.

## 3.1 Leaky Integrate-and-Fire (LIF)

In the introduction chapter, we have seen what an AP is and the general process for production; however, scientists have spent time trying to decode the information behind spikes. What we know is that the information and shape of a spike are generally the same, but the information lies in the presence or absence of an AP. Therefore, to utilize APs with the same form Louis Lapicque created the leaky Integrate-and-Fire (LIF) model [8, 20].

In the Neurophysiology & Neural Dynamics section 1.1, the momentary change of membrane potential of a neuron $i$ can be captured by a presynaptic AP, current injection $I(t)$, or with ion composition with the Nernst equation 1.1. In contrast, the resting membrane potential is characterized by the variable $V_{\text{rest}}$ when a neuron has not received any input. Therefore, the change in membrane potential can be measured as the difference between the current state of the neuron and its resting potential.

$$V = V_i(t) - V_{\text{rest}} \quad . \tag{3.1}$$

So, to derive the LIF, we apply the current $I(t)$ directly to the neuron inside the membrane walls, which acts as an insulator, and the additional charge from the electrode will alter the cell membrane.

$$q = \int I(t')dt' \quad . \tag{3.2}$$

Similarly to the derivation of the cable theory (Figure 7) for the axon, the electrical circuit set up for the LIF model consists of the membrane capacitor $C_m$ in parallel with the resistor $R_m$, with a current $I(t)$.

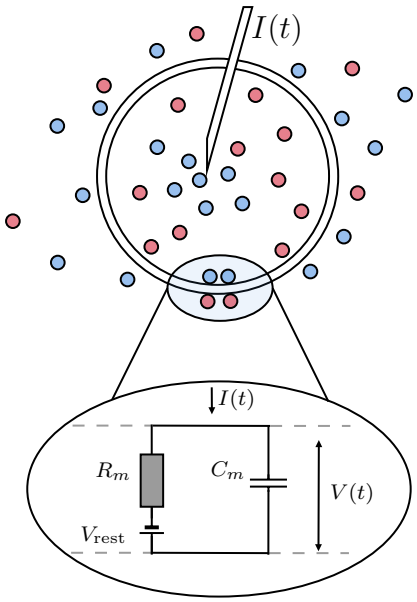


Figure 10: **Electrical circuit of a neuron injected with positive electrical input**. A passive neuron, enclosed by the membrane, receives a positive current $I(t)$ from the electrode, which increases the composition of positive charges (blue) inside the cell. The membrane walls act like a resistor $R_m$ in line with the battery at $V_{\text{rest}}$, and in parallel with the capacitor $C_m$. Figure replicated from [8].

Just as in the derivation of the cable equation, we treat our circuit as a standard RC circuit and analyze the current across the membrane, $I_m$. We use the law of current conservation to separate the current passing through the resistor ($I_r$) and capacitor ($I_c$).

$$I(t) = I_r + I_c \quad . \tag{3.3}$$

Using Ohm's law and the definition for the capacity, we rewrite to:

$$I(t) = \left(\frac{V_R}{R_m}\right) + \left(C_m \frac{dV}{dt}\right) \quad . \tag{3.4}$$

where $V_R$ is the difference between the voltage $V(t)$ and its resting potential $V_{\text{rest}}$. We multiply both sides by $R_m$, introducing the membrane time constant $\tau_m$:

$$R_m I(t) = (V(t) - V_{\text{rest}}) + \tau_m \frac{dV}{dt} \quad . \tag{3.5}$$

We substitute in the membrane potential definition $V$ (Equation 3.1), giving us the LIF model:

$$\tau_m \frac{dV}{dt} = -V + R_m I(t) \quad . \tag{3.6}$$

## 3.2 Neuronal Spike

We have derived an example of an external stimulus that contributes to the change in membrane potential in the previous section. However, neurons have a threshold for their membrane potential, known as the firing threshold. The resting membrane potential $V_{\text{rest}}$ sits at around $-75$ millivolts, but once they reach $-55$ millivolts, the neuron sends an AP to the postsynaptic neuron.

$$t^{(f)}: \qquad V\left(t^{(f)}\right) = \vartheta \quad . \tag{3.7}$$

where $\vartheta$ is the membrane potential threshold of $-55$ millivolts reached at time $t^{(f)}$.

To complete the LIF model, for $t > t^{(f)}$, the dynamics are reset back to the resting membrane potential $V_{\text{rest}}$.

$$\lim_{\delta \to 0; \delta > 0} V\left(t^{(f)} + \delta\right) = V_{\text{rest}} \quad . \tag{3.8}$$

With the combination of equations 3.6 and 3.8 we get the full dynamics of the LIF [8].

Additionally, the collection of spikes from neuron $i$ can be formulated by their times $t_i^{(f)}$, where $f$ is the spike number.

$$S_i(t) = \sum_f \delta\left(t - t_i^{(f)}\right) \quad . \tag{3.9}$$

This equation is also known as the firing rate for neuron $i$.

## 3.3 Field model derivation

From the LIF chapter, we derived Equations 3.6 and 3.8, which describe the dynamics of the membrane potential for an individual neuron in response to a postsynaptic spike or external stimulus, as well as its reset mechanism once the potential threshold reached -55 millivolts. Once a neuron reaches a threshold voltage, the neuron will fire and commence the process again [8].

In the field model depiction, we examine a population of neurons that are spatially connected and exposed to external stimulation after DES. To derive this new model, we build upon our understanding of the LIF model and extrapolate it to a population approximation using the mean-field theory (MFT) [22, 59]. The MFT approach will shift our perspective from an individual neuron to a high-dimensional average of groups of neurons.

Let us consider a network of excitatory and inhibitory LIF neurons that give rise to neuron $i$'s membrane potential. This means that each presynaptic neuron $j$ will stimulate neuron $i$ via presynaptic channels at a collection of time bins $t^{(k)}$. Therefore, the total synaptic input to neuron $i$:

$$I_{i,syn}(t) = \sum_j w_{ji} S_j(t) \quad . \tag{3.10}$$

where $w_{ji}$ is the synaptic weight of the synapse from neuron $j$ to neuron $i$, which is responsible for the strength of the spike. $S_j(t)$ is the firing rate for the different $j$ neurons in our network (Equation 3.9).

The first step in our MFT approximation is to assume a spatial arrangement for neurons to determine the mean firing rates of neurons in our network at each spatial location $\tilde{x}$ [22, 60].

$$\nu_j(\tilde{x}, t) = \langle S_j(t) \rangle_{x_j = \tilde{x}} \quad . \tag{3.11}$$

The following assumption is to take all the synaptic weights in the network and average them from the initial position $\tilde{x}$ to the connection at the next spatial location $x$ [59, 60].

$$\tilde{w}(\tilde{x}, x) = \langle w_{ji} \rangle_{x_j=\tilde{x}, x_i=x} \quad . \tag{3.12}$$

Thus, the synaptic mean current results in the convolution between synaptic kernel $\tilde{w}$ and the mean firing rate $\nu$ [59].

$$I_{syn}(x,t) = \langle I_{i,syn} \rangle = \int \tilde{w}(x - x') \cdot \nu(x', t) dx' = (\tilde{w} * \nu)(x,t) \quad . \tag{3.13}$$

Additionally to the synaptic mean current, we are evaluating the extracellular voltage induced by DES $V_{ext}$, providing us with the new and improved LIF model for DES, that incorporates an MFT synaptic current. Using equation 3.6 we get:

$$\tau_m \frac{dV(x,t)}{dt} = -V(x,t) + R_m (\tilde{w} * \nu)(x,t) + V_{ext}(x,0) \quad . \tag{3.14}$$

Where the extracellular voltage $V_{ext}$ caused by extracellular field during stimulation.

To summarize, we extended the LIF model from a singular neuron to a higher-dimensional, distributed network. We took the collection of synaptic inputs from individual neurons and averaged them spatially using MFT. This led to a spatially averaged LIF model, where the total synaptic current is now expressed as a convolution between the synaptic connectivity kernel and the mean firing rate [22, 59]. Additionally, we introduced the extracellular voltage evoked from the DES.

So far, the derivation of the spatially averaged LIF model is still homogeneous. However, cortical networks consist of two cell types, excitatory and inhibitory neurons, that interact in complex ways to shape the network dynamics [24, 59]. These neurons communicate with each other via synaptic channels; therefore, the synaptic current changes based on the communication. Thus, the communication ranges from excitatory to excitatory $e \to e$, inhibitory to inhibitory $i \to i$, excitatory to inhibitory $e \to i$, and inhibitory to excitatory $i \to e$, as shown in Figure 11.

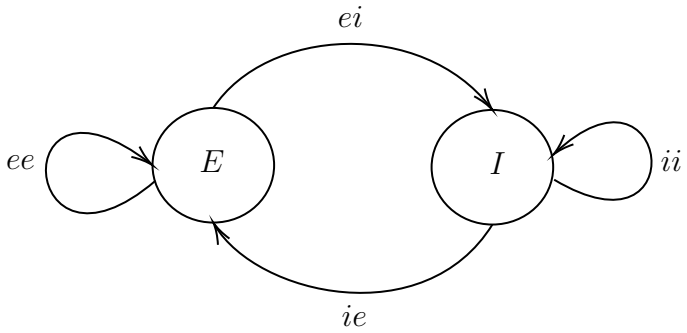


Figure 11: **Cortical recurrent connectivity**. A diagram depicting the interconnectivity between inhibitory and excitatory groups of neurons in the cortex. The excitatory to excitatory $ee$, excitatory to inhibitory $ei$, inhibitory to excitatory $ie$, inhibitory to inhibitory $ii$ synaptic connection [24].

Considering the role of excitation and inhibition in cell dynamics, we note that the excitatory cells produce a positive electric potential. In contrast, inhibitory cells produce a negative electric potential to inhibit other cells from firing [59]. Therefore, we can rewrite:

$$I_{e,syn}(x,t) = \tilde{w}_{ee}(x) * \nu_e(x,t) - \tilde{w}_{ie}(x) * \nu_i(x,t) \quad . \tag{3.15}$$

$$I_{i,syn}(x,t) = \tilde{w}_{ei}(x) * \nu_e(x,t) - \tilde{w}_{ii}(x) * \nu_i(x,t) \quad . \tag{3.16}$$

Combining everything, we get the evoked dynamics post-DES.

$$\tau_m \frac{dV_e}{dt}(x,t) = -V_e(x,t) + R_m \left((\tilde{w}_{ee} * \nu_e)(x,t) - (\tilde{w}_{ei} * \nu_i)(x,t)\right) + V_{ext}(x,0) \quad . \tag{3.17}$$

$$\tau_m \frac{dV_i}{dt}(x,t) = -V_i(x,t) + R_m \left((\tilde{w}_{ei} * \nu_e)(x,t) - (\tilde{w}_{ii} * \nu_i)(x,t)\right) + V_{ext}(x,0) \quad . \tag{3.18}$$

While other mean-field models collapse the excitatory and inhibitory dynamics into a single equation, we separate them to simulate their individual contributions to DES. Unlike traditional large-scale field models that assumes longer range of connectivity, we consider a different connectivity structure where synaptic kernel connections extend over hundreds of microns [11].

## 3.4 Initialization Regimes

We consider a field model of DES with a small number of parameters. The model aims to simulate the membrane potential, $V_e$ and $V_i$, of point neurons located in the space surrounding the electrode. We consider a single dimension ($x$) where $x = 0$ is the position of the electrode. The dynamics that follow direct electrical stimulation are modeled as

$$\tau_m \frac{dV_e}{dt}(x,t) = -V_e(x,t) + R_m \left( (\tilde{w}_{ee} * \nu_e)(x,t) - (\tilde{w}_{ei} * \nu_i)(x,t) \right) \quad . \tag{3.19}$$

$$\tau_m \frac{dV_i}{dt}(x,t) = -V_i(x,t) + R_m \left( (\tilde{w}_{ei} * \nu_e)(x,t) - (\tilde{w}_{ii} * \nu_i)(x,t) \right) \quad . \tag{3.20}$$

where $\nu_e = \Theta(V_e - \vartheta)$ and $\nu_i = \Theta(V_i - \vartheta)$ are the firing rates, taken to be a nonlinear readout, of excitatory and inhibitory populations, respectively (Definition $\Theta$ 7.4). The tissue is considered to have isotropic connectivity, modeled with a Gaussian connectivity [11], that is, the interaction kernels from excitation to excitation ($\tilde{w}_{ee}(x)$), from excitation to inhibition $\tilde{w}_{ei}(x)$, from inhibition to inhibition $\tilde{w}_{ii}(x)$ and from inhibition to excitation $\tilde{w}_{ie}(x)$ do not depend on the point of origin. More on Parameters in the next chapter 3.5.

Our model of the direct electrical effect affects the initial conditions of the membrane potential $V_i(x,0)$ and $V_e(x,0)$, such that $t = t_i$ is the time of the microstimulation. It is equivalent to adding terms to Eqs. 3.19-3.20 equal to

$$\delta(t - t_i)V_e(x,0) \qquad \text{and} \qquad \delta(t - t_i)V_i(x,0) \quad . \tag{3.21}$$

These equations reflect an instantaneous voltage shift at the time of stimulation. Here, we considered two models, which we referred to as the *depolarization* and *activation* models which reflect Stoney's direct stimulation of the pyramidal tract cells and Histed's activation of passing axons respectively.

### 3.4.1 Depolarization Model

The depolarization model reflects the activation seen in Stoney and colleagues by directly stimulating neurons, for the spatial profile at the moment of stimulation, the direct electrical effect $k$ depolarizes the membrane potentials of cells as a power-law approximation of distance to the electrode [12, 13].

$$V_e(x,0) = \frac{RI}{(x+\alpha)^p} \quad \text{and} \quad V_i(x,0) = \frac{kRI}{(x+\alpha)^p} \quad . \tag{3.22}$$

where $I$ is the stimulation intensity, $R$ is the resistance of the electrode to the neuron, $\alpha$ is the offset parameter, and $p$ controls the power-law function (typically, $p = 2$ [12, 13]). The parameter $k$ allows us to control the relative amount of direct electrical effect in excitatory vs inhibitory populations [23].

### 3.4.2 Activation Model

The activation model reflecting Histed and colleagues findings, we initialize the electrical stimulation to trigger AP firing in nearby axons, resulting in a sparse, distance-dependent depolarization of the tissue:

$$V_e(x,0) = 0 \; ; \; \nu_e(x,0) = \gamma_e \cdot log(I) \cdot \mathcal{N}(x|\sigma^2_{e,stim}) \quad . \tag{3.23}$$

$$V_i(x,0) = 0 \; ; \; \nu_i(x,0) = \gamma_i \cdot log(I) \cdot \mathcal{N}(x|\sigma^2_{i,stim}) \quad . \tag{3.24}$$

Where $\log(I)$ is the nonlinear stimulation intensity; meaning, that as the stimulation intensity increases there is no continuous recruitment of nearby axons as it was seen in Histed's findings [14]. The $\gamma_e$ and $\gamma_i$ are gain parameters that scale in amplitude of $e$ and $i$ activation. The $\sigma_{e,stim}$ and $\sigma_{i,stim}$ define the spatial spread of stimulation via normalized Gaussian $\mathcal{N}(x|\sigma^2)$, representing the likelihood of axons pass close enough to the electrode for electrical stimulation to be activated.

We assume that the primary effect of stimulation is to induce axonal spiking, which corresponds with experimental findings that direct activation of axons dominates the response to stimulation [9]. We specifically consider induced APs and treat axon and soma-driven firing into a single distance-dependent firing probability.

## 3.5 Parameters

This section provides a more in-depth examination of the various parameters that influence the field models and the types of amplifications elicited from parameter tuning. In the previous chapters, we introduced these variables without too much context on their operation and how they can affect the state of the spatial spread post-DES.

In the following, we will be breaking down the spatial configurations of the synaptic kernels. We will see that they are constructed into two functionalities: the synaptic weight and the one-dimensional Gaussian spatial spread. Additionally, the direct electrical effect from the depolarization model, and its connection to cable properties must also be described.

### 3.5.1 Synaptic Scale $W$ & Connection Probabilities $\sigma$

In our formulation of the field model in 3.17-3.18, the synaptic kernels $\tilde{w}_{\alpha,\beta}(x - x')$ represent spatially distributed connectivity between the groups of $e$ and $i$: $e \to e$, $e \to i$, $i \to e$, and $i \to i$. Each kernel consists of two components: a synaptic weight $W_{\alpha,\beta}$ and a normalized Gaussian $\mathcal{N}(x|\sigma^2)$.

The first part is the synaptic weight scaling parameter. The purpose of this parameter is similar to that of the gain parameter in the activation model, which is to amplify connections between populations of $e$ and $i$. A higher synaptic strength increases the likelihood of a population of group $\alpha$ influencing a population of group $\beta$.

The normalized Gaussian with a spatial spread of $\sigma$'s serves to establish spatial connectivity between population groups of $e$ and $i$, meaning that a higher synaptic connection increases the likelihood of connections between two groups at a greater intersomatic distance compared to a smaller connection, which is consistent with experimental observations [11]:

$$\tilde{w}_{\alpha\beta}(x - x') = W_{\alpha\beta} \cdot \mathcal{N}(x - x'|\mu = 0, \sigma^2_{\alpha\beta}) \quad | \quad \alpha, \beta \in \{ee,\ ei,\ ie,\ ii\} \quad . \tag{3.25}$$

It is important to note that we are working within a one-dimensional over position where the origin is represented as the electrode; meaning, the normalized connections follow a half-Gaussian distribution centered at the origin. Implying that connectivity and activity probability are higher near the electrode and decrease as the distance increases between the groups and the electrode.

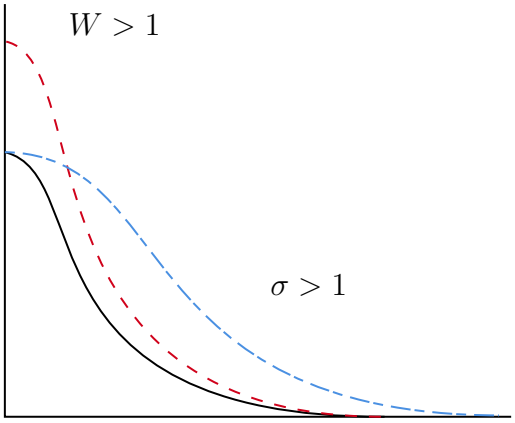


Figure 12: **One-dimensional effect of synaptic weight and spatial spread**. This plot shows the synaptic kernels under three configurations, where the abscissa is the distance $x$ away from the electrode at the origin, and the ordinate is the synaptic coupling strength. The baseline kernel (black), the synaptic strength $W > 1$ (red) raises the amplitude, and the spatial spread $\sigma > 1$ (blue) extends the connectivity profile.

### 3.5.2 Direct Electrical Effect $k$

Previously, we covered the three possible outcomes following cortical DES: the non-amplified case, where the induced cortical activity following the stimulus decays immediately to its equilibrium state. Second, the runaway amplification case, where DES could result in a runaway expansion and potentially lead to seizure-like patterns. Lastly, the transient amplification case, where there is an amplification from the direct effect of stimulation that returns to the baseline state. The importance of the direct electrical effect $k$ from the depolarization model is based on these three possible outcomes. The definition of the variable is the ratio of activation between the $e$ and $i$ groups.

$$k = \frac{k_i}{k_e} \quad . \tag{3.26}$$

Here, $k_e$ and $k_i$ represent the fraction of the excitatory and inhibitory populations activated directly by the stimulus.

Following this equation, in the non-amplified case, $k \approx 1$, the ratio of activation to inhibition is roughly equal, resulting in a balanced response. In other words, we have recruited the same amount of excitation and inhibition from our stimulation, resulting in a brief activation followed by a decay back to equilibrium.

For the runaway expansion, the ratio $k \to 0$, which would entail that there is more excitatory recruitment and nearly no inhibition that has been recruited.

Lastly, the transient amplification, $0 < k < 1$, occurs when the direct effect of inhibition is less than the excitatory effect.

The ratio of inhibition and excitation is based on the proportion of the affected population in that group.

# 4 Results

In this chapter, we present the results obtained through the various methods employed in Sections 2 and 3. We will first introduce our findings on axonal activation, which primarily utilize information derived from the intensity threshold distribution. We will use this information to discuss the bias recruitment from stimulation and the reasoning behind needing inhibitory myelination for the recruitment of excitatory units for transient amplification.

Following the axonal activation, we will relate the axonal $e$ and $i$ recruitment imbalance to the direct electric effect $k$ seen in the depolarization model. This supports our central hypothesis that imbalanced recruitment from axonal activation can lead to transient amplification.

Lastly, we will conclude with the activation model, distinguishing between the two models while highlighting parallel similarities in obtaining similar network-level responses. Most importantly, the chapter will confirm our hypothesis that the imbalanced recruitment from axonal activation can lead to transient amplification.

For simplicity, we set the resting membrane potential $V_{rest}$ as the reference point in our plots. This enables us to set the threshold voltage $\vartheta$ at 20 millivolts.

## 4.1 Axon Activation

In the Cable Properties section (Section 2), we derived the cable equation, which describes how voltage propagates along axons and dendrites as a function of their electrical properties. This introduced us to the biophysical quantities such as membrane resistance, capacitance, and electric constants. Building on this, we used the strength-intensity curve definition to find a relation between chronaxie and diameter based on experimental and derivational findings [9, 25].

On average, excitatory neurons tend to have slightly thinner axon diameters compared to inhibitory axons [10, 26]. Although they partially overlap, we investigated whether this subtle difference could lead to biased recruitment when the subjects are stimulated. We derived an equation that relates the intensity thresholds to the axonal diameters through the strength-intensity equation. Since axonal diameter distribution tends to be normally distributed, we used variable change methods to find the probability distribution function for the intensity threshold. This results in a distribution of threshold currents (Figure 13**c**), where a similar overlap persists.

At a fixed stimulation intensity, the likelihood for an axon to be recruited depends on whether its threshold current is below the stimulation amplitude. Thus, the stimulation intensity will result in a fraction of activated axons that can be used to determine the network response in the field model due to the imbalance of the excitatory and inhibitory populations.

While considering the distribution of the intensity threshold, we observe that inhibitory axons are more likely to be activated, due to their larger diameters, at lower amperages compared to excitatory axons, resulting in a significantly greater ratio of inhibition than excitation. However, at larger amperages, both populations approach full activation, and the I/E recruitment ratio converges to 1.

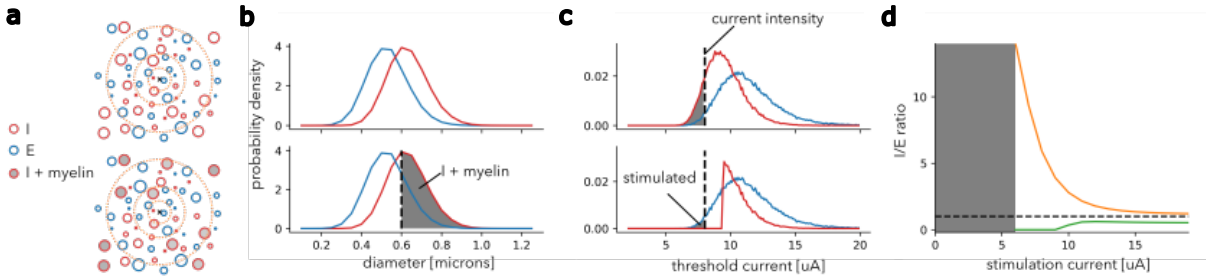


Figure 13: **Statistical cable differences implies recruitment bias**. **a-c** Considering statistical differences in axon morphologies for excitation (E) and inhibition (I) within a non-uniform electric field. Top row shows a case where excitation has thinner axon diameters than inhibition. Bottom row shows a case where, in addition to the difference in diameters, I cells also have myelinated axons but only for the thicker axons. **b** Distribution of axon diameters. **c** Associated distribution in threshold currents. The threshold currents for myelinated fibers fall outside of the range shown. **d** Resulting recruitment ratio calculated with distance-dependent electric field is shown for the diameter-only distinction (orange line) and the diameter without myelin distinction (green line). This figure was generated by Richard Naud and used in this thesis with his permission.

Therefore, in order to obtain transient amplification, we need to explore conditions under which we can obtain an excitatory bias. We consider the possibility that only large inhibitory neurons are myelinated (Figure 13**b**, bottom). In this case, the threshold current for the larger inhibitory axons is very large due to the myelin sheath acting as an insulator, preventing lower threshold currents from activating them. This truncates the inhibitory recruitment curve (Figure 13**c**, bottom), allowing smaller currents to recruit excitation before inhibition, resulting in the overall recruitment ratio being dominated by excitation (Figure 13**d**, green). This bias persists across a range of intensities because myelinated inhibitory axons remain unresponsive unless much larger currents are at play.

This model was motivated by experimental observations of parvalbumin-positive cells, a class of inhibitory neurons found in the cortex. These cells are shown to receive extensive myelination on their larger-diameter axons [27, 26]. However, in contrast to inhibition, the myelination of excitatory neurons is more complex and depends on the cortical layer and post-synaptic target [28].

## 4.2 Depolarization Model

In the previous chapter, we derived the field model equations 3.17-3.18, which should describe the behaviour of a network of excitatory and inhibitory groups, interconnected via synaptic coupling that is Gaussian distributed, when faced with DES. To initialize the problem, we have derived that the activation begins with dipolar electrode stimulation, which is controlled by the intensity of the probe and the resistance from the electrode to the cell (Equation 3.22).

The depolarization model is a one-dimensional field model where the electrode is positioned at the origin, $x = 0$, delivering a stimulation. In the results, we chose a dipolar potential that stimulates, $I_o = 500\mu A$, a population of excitatory neurons and half the inhibitory population, $k = \frac{1}{2}$. The synaptic weights chosen in this model adhere to density and number of synapses, which are dominated by excitatory coupling rather than inhibitory connections [24]. This is done while maintaining the spatial spread equally distributed for all connections $\sigma = 150\mu m$.

| parameter | value | units |
|---|---|---|
| $I_o$ | 500 | $\mu A$ |
| $W_{ee}$ | 230 | a.u. |
| $W_{ie}$ | 150 | a.u. |
| $W_{ei}$ | 150 | a.u. |
| $W_{ii}$ | 25 | a.u. |
| $\sigma_{ee}$ | 150 | $\mu m$ |
| $\sigma_{ie}$ | 150 | $\mu m$ |
| $\sigma_{ei}$ | 150 | $\mu m$ |
| $\sigma_{ii}$ | 150 | $\mu m$ |
| $k_i$ | 0.5 | a.u. |
| $k_e$ | 1 | a.u. |

Table 1: **Parameters from the depolarization model that evoke transient amplification**. For the depolarization model initiation, we have set the initial intensity to $500\mu A$, and the direct electric effect on inhibition reduced to half of its population. For the field model, we maintained an equal spatial spread $\sigma$ while scaling the synaptic weights according to the communication patterns observed in cortical circuits.

From the list of parameters in Table 1, to obtain transient amplification, the initialization for the depolarization would require us to create a bias of leading excitation and lagging inhibition. The focal point of the imbalanced start stems from the inhibitory direct electrical effect $k_i = 0.5$, which implies a weaker electrical effect on inhibitory cells,

while maintaining the full electrical effect on excitatory cells $k_e = 1$.

Additionally, from a higher-dimensional perspective, if the increase of intensity results in more axonal recruitment, this would imply that the imbalanced start comes from the bias in axonal recruitment; meaning, the ratio of activation found in the green curve of Figure 13**d** correlates with the direct electric effect. Therefore, the excitatory and inhibitory cable properties do control the transient amplification of electrical stimulation.

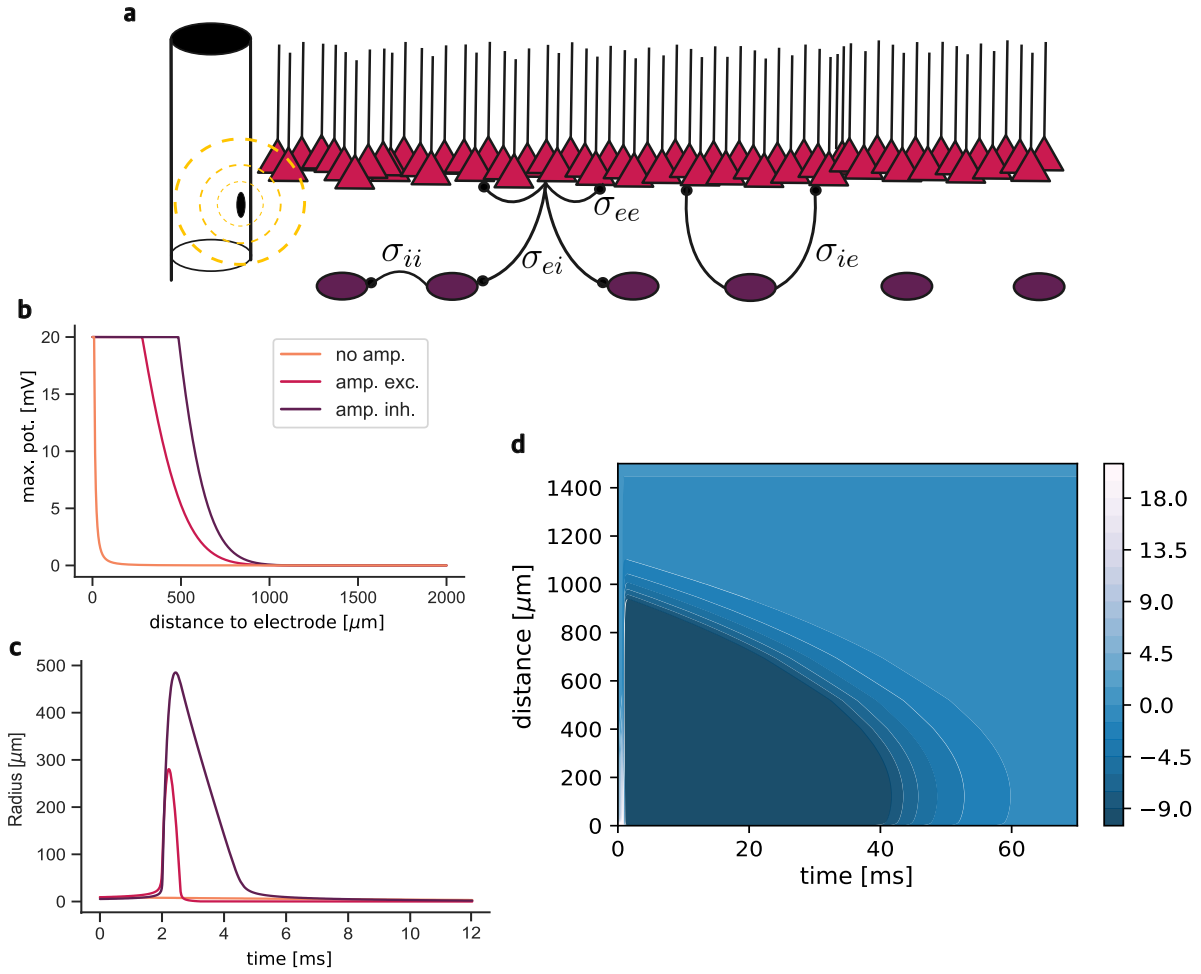


Figure 14: **Network structure of depolarization model**. **a** A one-dimensional field model of excitation and inhibition receiving localized direct stimulation using equations 3.17-3.18 with the initializations of equation 3.22. Coupling between cells is provided by a Gaussian kernels characterized by fixed $\sigma = 150\mu m$. **b** Maximum (timewise) potential as a function of distance. The orange line corresponds to a model without any amplification. The red (excitatory) and purple (inhibitory) lines correspond to a model where direct stimulation of inhibition is half that of excitation. **c** Radius of activated units as a function of time. **d** Membrane potential heatmap of depolarized units going through action potentials over time and space.

The results in Figure 14**bc** show that through the parameters, in Table 1, we were able to propagate the excitatory signal 300 microns away from the stimulation site in 2

milliseconds. Once the excitatory units started charging the inhibitory units, the inhibition quickly caught up at 500 microns. It overtook the excitation in microseconds, then suppressing the excitatory signal enough that excitation could no longer expand. Meanwhile, if there were no bias towards ($k_i = 1$), then we see that there was no propagation of the signal. That means that at the time of stimulation, the inhibition was already strong enough to inhibit the excitation, leading to a non-amplified case.

We can see a different perspective on the network's behaviour at the moment of stimulation in Figure 14**d**. At the 5 millisecond mark, we see many cells going through depolarization and firing APs in the first 500 microns. Following this, there is an immediate hyperpolarization refractory period from the original units, followed by inhibition, and a prolonged recovery period to return to the resting state. Thus, we can see the similarities between the membrane potential heatmap and the **bc** plots.

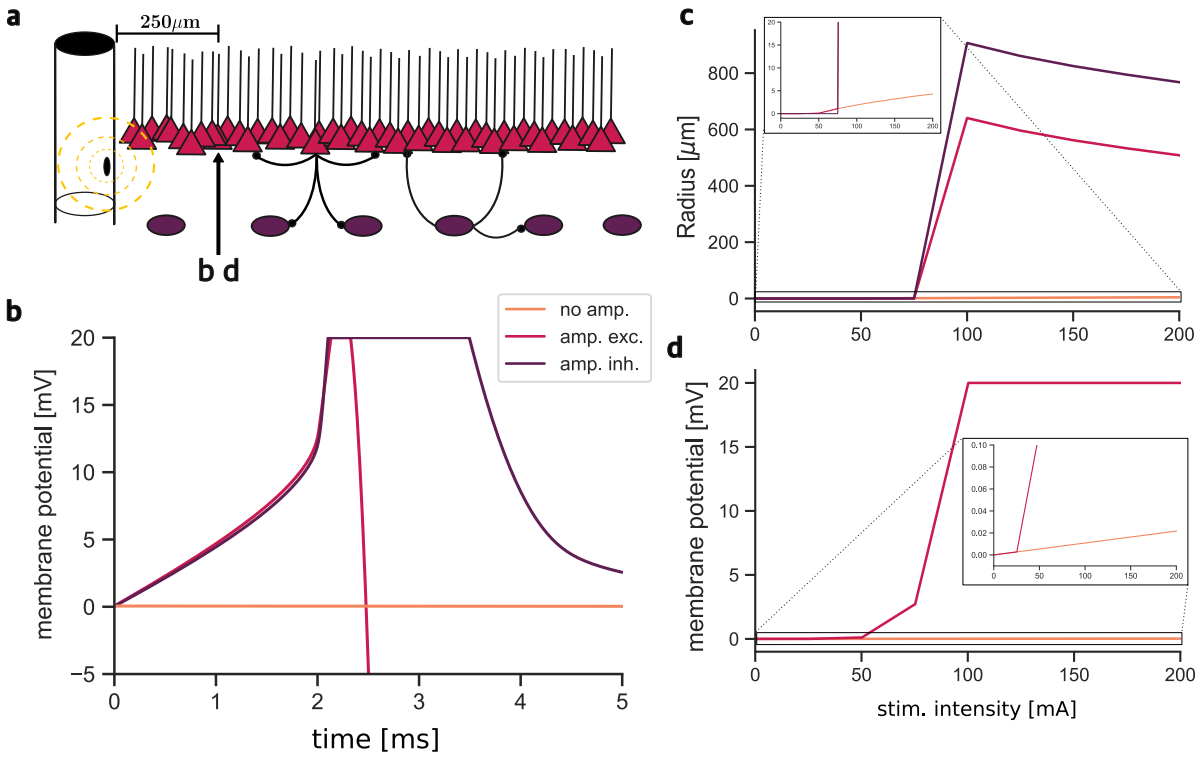


Figure 15: **Depolarization from a reference point**. **a** Again a one-dimensional field model through positional frame of reference of $x = 250\mu m$ away from the localized direct electrical effect $x_0$. **b** Maximum (timewise) potential as a function of time. The orange line corresponds to a model without any amplification. The red (excitatory) and purple (inhibitory) lines correspond to a model where direct stimulation of inhibition is half that of excitation. **c** Radius of activated units as a function of stimulation intensity. **d** Maximum (timewise) potential as a function of stimulation intensity.

From Figure 15**a**, we take a readout point 250 microns away from the electrode in the one-dimensional picture. After initializing the depolarization model, we observe a gradual increase in membrane potential at the reference point (Figure 15**b**), with excitation leading and inhibition lagging, demonstrating the transient amplification. Eventually, the units at the reference point reach their threshold potential due to the synaptic inputs, and they fire together. At the threshold, the excitatory units fire for a quarter of a millisecond, while the inhibitory units fire for approximately a millisecond. Once excitation finishes firing, we can observe a plunge in membrane potential due to regular hyperpolarization, as well as the inhibitory units hindering the excitatory units through the synaptic kernels $\tilde{w}_{ie}$. The decline of excitation is soon followed by a decline of inhibition due to natural hyperpolarization and inhibitory synaptic kernels $\tilde{w}_{ii}$. Once all the excitatory neurons in the network have stimulated the inhibitory neurons to the point of firing, the inhibitory neurons will eventually stop stimulating other cells in the network, allowing for a gradual refractory period back to the steady state.

In addition to monitoring the membrane potential change due to the field model, we want to know the influence of intensity on the network. This will enable us to determine the radius of activated units by gradually increasing stimulation intensity, also known as the r-I curve (Figure 15**c**). As we increase the intensity, we expect an increase in volume. Stoney and colleagues proposed that the volume of somatic activation increases with the square root of stimulation intensity [12, 13]. In our case, the r-I curves, with the parameters in Table 1, do not validate Stoney's predictions. Instead, there is a decline in radial unit activation as intensity continues to rise. That happens because the network is now saturated with more inhibitory activation, resulting in inhibition that overcomes excitation. However, in the non-amplified case (orange line), there is a slow and gradual increase in spatial expansion due to the increasing stimulus, which may correspond with Stoney's hypothesis.

Finally, Figure 15**d** provides the reference point for the increase in membrane potential as stimulation increases. From 250 microns away, lower intensities do not derive the excitatory components to spike. Nevertheless, once larger inputs dominate the dynamics, there is an increase in the membrane potential for both amplified and non-amplified cases. While the non-amplified case slowly increases, the amplified cases have already reached the threshold (Table 1).

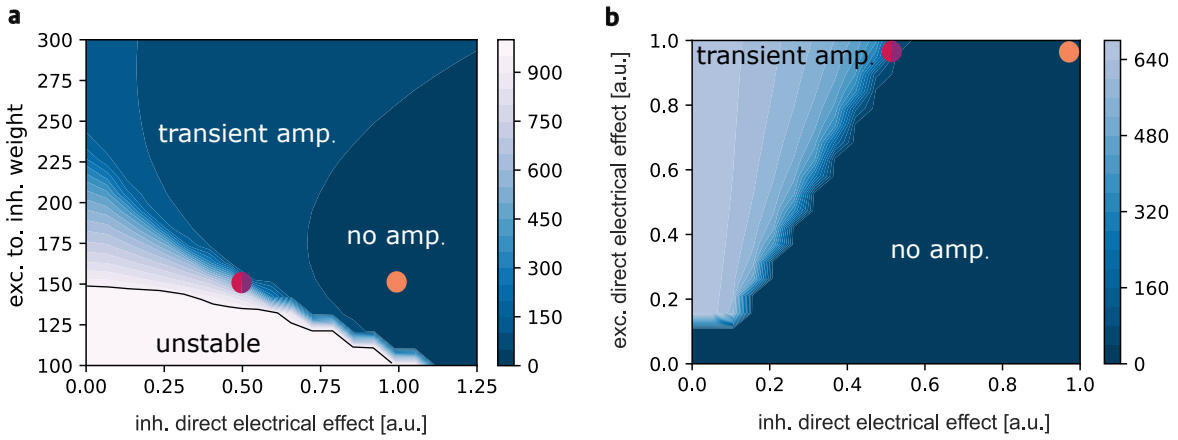


Figure 16: **Depolarization and network responses**. Both heatmaps show the maximum activated radius reached by excitation for the depolarization model. The orange point denotes the model parameters used for the model with no amplification. The red/purple point denotes the parameters used for the model showing transient amplification in the rest of the figures. **a** Heatmap evaluating the synaptic weight of excitation onto inhibition and the ratio of direct stimulation of inhibition. **b** Heatmap evaluating the ratios between the direct stimulation effect from excitation and inhibition.

Additionally, we conduct a grid search over key parameters to identify regions of stable, unstable, and transient dynamics within the network. The results indicate a potential for reaching unstable regions that would continuously propagate excitatory signals unchecked by inhibition. This resembles an epileptic attack, where recurrent excitation is no longer inhibited, causing cells to fire continuously [56]. On the other extreme, we have a system with no amplification, meaning the signal did not have a chance to propagate due to inhibition. Between these two zones, we see, in Figure 16ab, the transient amplification zone that we selected using the parameters in Table 1, which supports temporary propagation of excitatory activity, then balanced by the delayed inhibitory recruitment. From these plots, we can infer the approximate spatial radius of activation under different parameter regimes.

## 4.3 Activation Model

In contrast to the depolarization model, which assumes the localized direct somatic depolarization, as seen in studies by Stoney et al [12], the activation model focuses on the network-evoked responses by stimulating the neuropil, which recruits the majority of passing axons. The model follows Histed's findings that suggest that increasing current primarily leads to the activation of passing axons more than nearby cell bodies [14].

The initiation of the activation model begins with stimulus-induced axonal spiking, resulting in a sparse and spatially distributed depolarization of the tissue. The initialization of the field model starts with the firing rate proportional to the scaled likelihood of axonal recruitment. We do not stimulate extracellular voltage into our model. Instead, the potential from the electrode occurs at some distance away from our field model, and the influx of activity into our field model results from axonal and somatic APs that drive our field model to different network outcomes.

| parameter | value | units |
|---|---|---|
| $I_o$ | 500 | $\mu A$ |
| $W_{ee}$ | 600 | a.u. |
| $W_{ie}$ | 400 | a.u. |
| $W_{ei}$ | 600 | a.u. |
| $W_{ii}$ | 150 | a.u. |
| $\sigma_{ee}$ | 127 | $\mu m$ |
| $\sigma_{ie}$ | 99.6 | $\mu m$ |
| $\sigma_{ei}$ | 99.84 | $\mu m$ |
| $\sigma_{ii}$ | 126.77 | $\mu m$ |
| $\sigma_{i,stim}$ | 127 | $\mu m$ |
| $\sigma_{e,stim}$ | 127 | $\mu m$ |
| $\gamma_i$ | 150 | a.u. |
| $\gamma_e$ | 600 | a.u. |

Table 2: **Parameters from the activation model that evoke transient amplification**. For the activation model initiation, we have set the initial intensity to $500\mu A$, and the inhibitory scaling parameter to the quarter of excitatory gain, while maintaining the spatial spread from stimulation $\sigma_{stim}$ the same. We set connectivity profile according to experimental connection probabilities found in mice [11]. while scaling the synaptic weights according to the communication patterns observed in cortical circuits [24].

From the list of parameters in Table 2, we wanted to obtain a transient amplified network response. Similarly to the depolarization model, we chose parameters that would initiate an excitatory/inhibitory imbalance ($\gamma_e > \gamma_i$). This imbalance controls the magnitude of the mean rate influx entering our field model.

We have decided to maintain the spatial spread $\sigma_{stim}$ of activation similar for both excitatory and inhibitory populations. We introduced an imbalance in the synaptic spatial kernels ($\sigma$) based on experimental observations by Campagnola et al. [11], which indicate broader excitatory than inhibitory connections.

Finally, the synaptic weights $W$ were assigned according to the communication patterns observed in cortical circuits, where the aggregate excitatory-to-excitatory connectivity is generally stronger than inhibitory connections due to higher synapse numbers and density [24].

Conceptually, this imbalance is similar to the link established between axon activation and the depolarization model. In both cases, biasing excitation over inhibition creates a window for transient amplification. In the activation model, contrary to the previous sections, we do not apply a direct extracellular voltage to the field model; instead, we use input from somatically and antidromically activated axons from DES to stimulate and activate our field model.

The following figures illustrate amplified, non-amplified, and unstable network responses resulting from indirect stimulation of the field model.

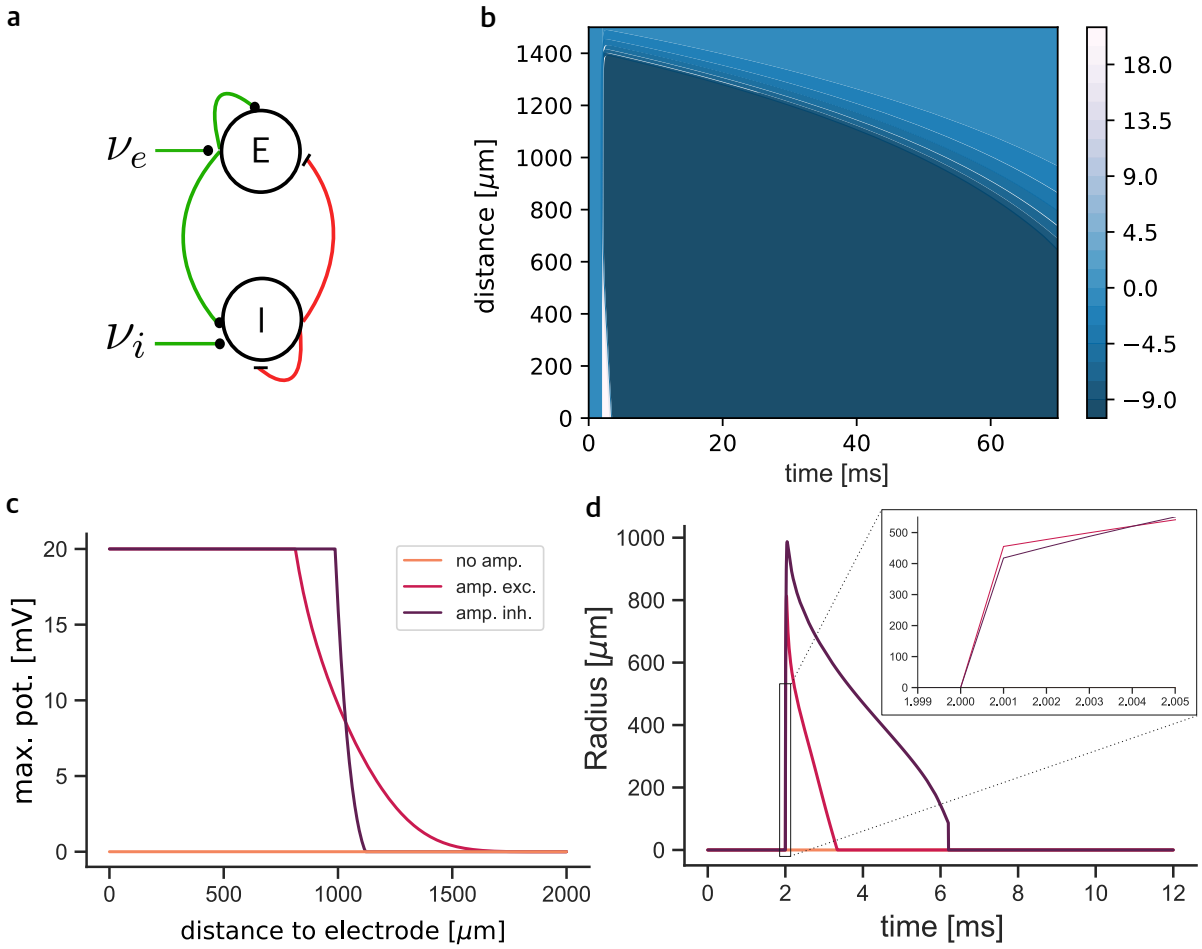


Figure 17: **Transient amplification from indirect stimulation**. **a** A field model of local excitatory (top) and inhibitory (bottom) dynamics across cortical space receiving feed-forward excitatory and inhibitory rate that was activated from indirect electrical stimulation using equations 3.17-3.18 with the initializations of equations 3.23-3.24. **b** Membrane potential heatmap of depolarized units going through action potentials over space and time. **c** Maximum (timewise) potential as a function of distance. The orange line corresponds to a model without any amplification. The red (excitatory) and purple (inhibitory) lines correspond to a model where the likelihood scale is a quarter that of excitation. **d** Radius of activated units as a function of time.

In Figure 17**b**, we visualize the spatiotemporal evolution of membrane potential across the field model. In the first 2 milliseconds, the network was at rest. Then, it undergoes a sudden spur of activation, with the membrane potential reaching threshold voltages at distances of a millimeter away from the origin. After 6 milliseconds, spiking stops, and a network-wide hyperpolarization occurs for the units closest to the received input. The system then returns to steady state sometime after 80 milliseconds.

Figure 17**cd** proves that the parameters selected in Table 2 lead to the transient amplification in the excitatory (red) and inhibitory (purple) units. We observe the signal from the excitation propagating to $800\mu m$ until inhibition catches up to halt the expansion at $1000\mu m$. This outcome is due to the mean rates of activation from the antidromic

axons and somas, creating a runaway signal for the excitatory population. However, the communication of the excitatory-to-inhibitory coupling is so strong that it gives inhibition time to catch up within microseconds to overtake the excitation. This demonstrates another example of transient amplification.

In the non-amplified case (orange), we notice that the model exhibits no reaction to the balanced rates ($\nu_e < \nu_i$), resulting in a flat line, as the inhibition in the field model already affects the excitatory units before they can rise. This is contrary to the depolarization model, where we never see a potential fall-off, as shown in Figure 14**b**, due to the direct extracellular potential perturbing the membrane.

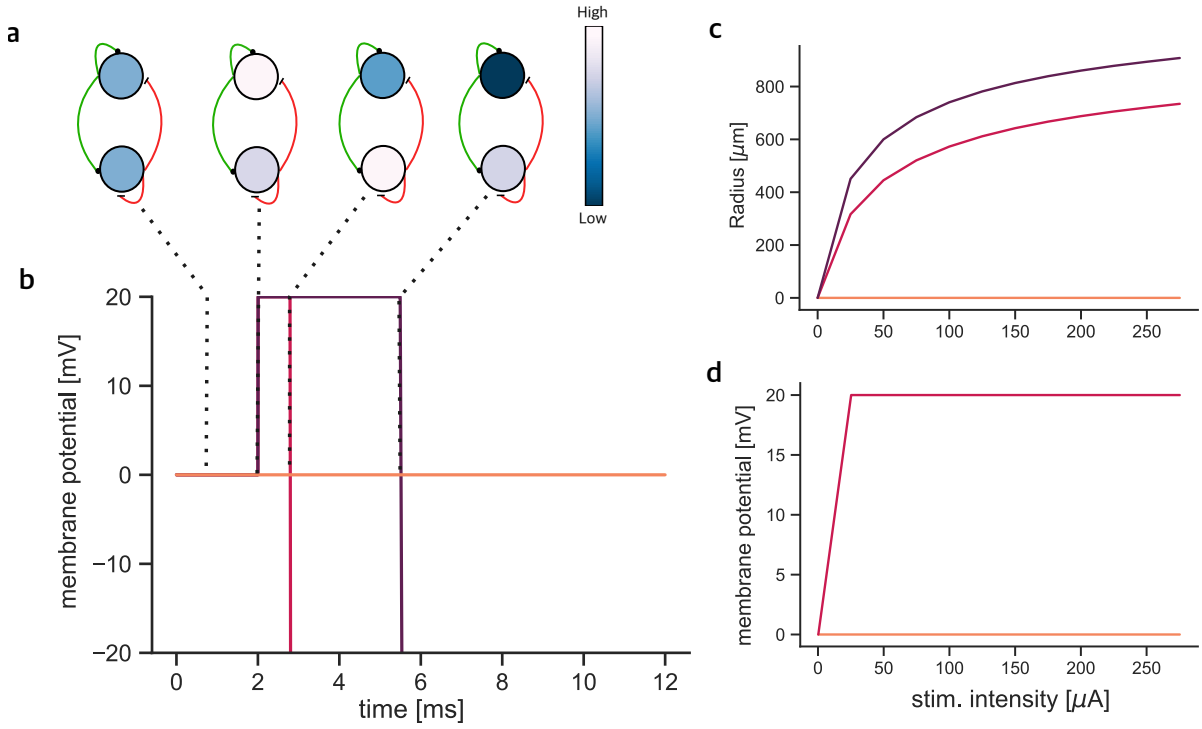


Figure 18: **Activation model from a reference point**. **a** The maximum potential for excitatory (top) and inhibitory (bottom) units at $x = 250\mu m$. Blue units indicate resting membrane potential at the system-level. Light-blue units indicate some depolarization across the population. White units indicate firing. Dark units indicate hyperpolarization. **b** Maximum (timewise) potential at $x = 250\mu m$ as a function of stimulus intensity. **c** Maximum activated radius as a function of stimulus intensity. **d** Potential at $x = 250\mu m$ as a function of time.

In Figure 18**a**, we take the perspective of excitatory (top) and inhibitory (bottom) populations about 250 microns away from the point of origin and take the membrane potential readout as the propagating signal reaches them. From Figure 18**b**, the membrane potential is not yet perturbed from the presynaptic colonies ahead of them, resulting in our units remaining at rest (blue circles). At around 2 milliseconds, the excitatory

membrane potential induced by the presynaptic population reaches the threshold voltage (white circle), while inhibition lags (light-blue). After a millisecond, excitation begins to decline rapidly (dark blue), while inhibition continues to fire (white). Two milliseconds after excitatory units started hyperpolarizing (dark), inhibition starts to decline rapidly (blue circle). This illustrates another instance of transient amplification in the excitatory (red) and inhibitory (purple) using the activation model.

The r-I curve (Figure 18**c**) characterizes the spatial spread of activation from the indirect stimulation, resembling a logarithmic growth as intensity increases in our model. This makes sense given that the synaptic mean rates are proportional to the logarithm of intensity ($\log(I_o)$). As a result, lower intensities recruit many passing axons, leading to a greater increase in spatial activation. Contrary to low intensities, high intensities recruit more distant axons due to most of the low-threshold axons already being recruited, leading to a slower growth in spatially activated units. The logarithmic scaling is consistent with experimental observations in ICMS, corresponding phenomenologically to the sparse spatial activation found in Histed et al [14].

Lastly, Figure 18**d** provides the reference point for the increase in membrane potential as stimulation increases. From 250 microns away, it only takes $25\mu A$ from the indirect stimulation to recruit enough passing axons to evoke threshold voltages onto the population.

The transient evoked responses from the system arise from the bias in the initial activation, specifically in the imbalance in the excitatory to inhibitory scaling parameters ($\gamma_e > \gamma_i$). However, in any of the cases where inhibitory rates are equal to or greater than the excitatory rates ($\nu_i \geq \nu_e$), we obtain no amplification (orange) in our model.

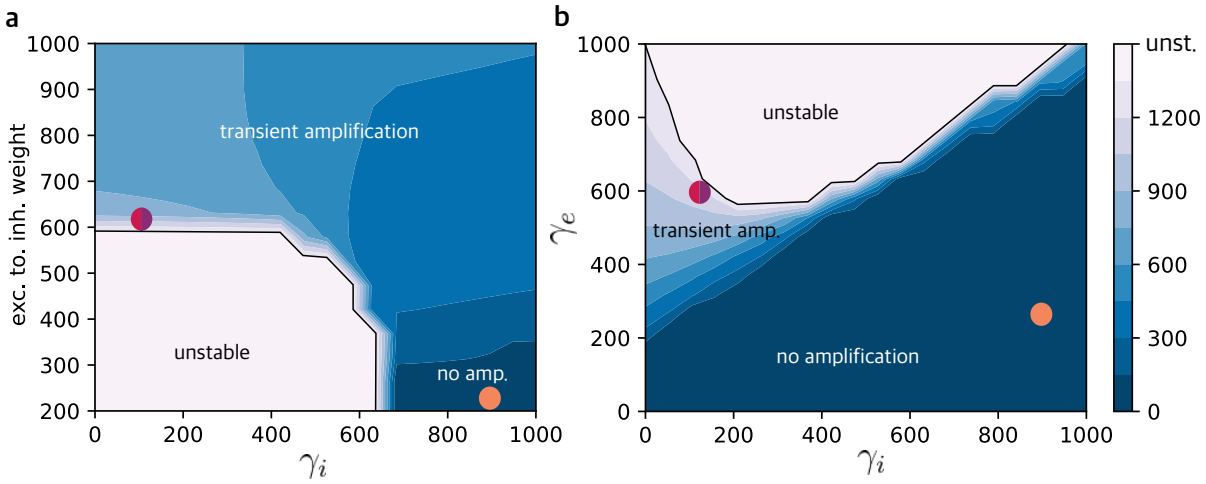


Figure 19: **Parameter searching for activation model**. Both heatmaps show the maximum activated radius reached by excitation for the activation model. The orange point denotes the model parameters used for the model with no amplification. The red/purple point denotes the parameters used for the model showing transient amplification. **a** Heatmap evaluating the synaptic weight of excitation onto inhibition and the inhibitory gain. **b** Heatmap evaluating the scale between excitation and inhibition.

Additionally, we conduct a grid search over key parameters to identify regions of stable, unstable, and transient dynamics within the network for the activation model. Similarly to the findings in the depolarization model, the results suggest that a potential exists for reaching unstable, transiently amplified, and non-amplified regions within the parameter spaces in Figure 19**ab**. With the parameters we chose in Table 2, we remain outside the unstable regions, allowing for the temporary propagation of excitatory activity, which is then balanced by the delayed inhibitory recruitment. From these plots, we can infer the approximate spatial radius of activation under different parameter regimes.

Figure 19**b** provides an interesting perspective on the scaling parameters that influence the outcomes of the mean firing rate in the no-amplification region. If $\gamma_i \geq \gamma_e$, the majority of the network would fall in the no amplification region. However, some regions of the network show a promising probability for runaway expansion in the field model when $\gamma_i \geq \gamma_e$. Nonetheless, for the most part, $\gamma_e > \gamma_i$ for transient amplification.

This imbalance from the gain parameters suggests a bias from the direct electric effect in the neuropil, which causes more excitatory activation than inhibition, leading to a transient amplification in our network.

# 5 Discussion

Intracortical microstimulation can be used to restore neural circuits in patients who have lost somatosensory responses, thereby moving away from the very invasive nature of deep-brain modulation techniques. However, the current understanding of intracortical microstimulation is controversial among scientists, and there remains no objective consensus on the evoked spatiotemporal responses from cortical stimulation. In our thesis, we aimed to understand how differences in axonal cable properties affect the spatiotemporal dynamics of stimulation in the cortex.

To address this, we have analytically derived a mapping from axon diameter in the cortex. Then, we derived a field model involving a network of leaky integrate-and-fire neurons that were interconnected and recurrent, and applied the mean-field approximation to obtain population-level dynamics. By understanding the recruitment behaviour of electrical stimulation, we highlighted the initial excitatory and inhibitory imbalance that would cause runaway excitation followed by inhibitory overtake.

Both field models that we have created, which differ in initialization, have reproduced key features of transient amplification, which begins with an imbalance in excitatory and inhibitory activations. In addition to transiently amplified networks, we have shown non-amplified and unstable networks that can arise from improper parameter tuning.

In the following sections, we will explore the biological implications of axonal cable properties and their relationship to the depolarization model and the activation model, which considers both antidromic axonal and somatic activation. Then, we will explain the limitations of the models. Lastly, we will discuss future work in addition to the current thesis project.

## 5.1 Biological Implications

The results of this study reveal several crucial biological implications for how the cortex responds to electrical stimulation, particularly regarding the wiring and the imbalance between excitation and inhibition. By incorporating realistic biophysical parameters, our model reveals that, in response to a subtle statistical difference, the stimulation can elicit three distinct responses: non-amplified, transiently amplified, and unstable.

First, we established a relationship between axonal diameters and the intensity threshold. On average, based on experimental data (Micheva, Kristina D., et al., 2016), show that inhibitory axons are larger in diameter than excitatory axons [10]. This implies that inhibitory axons are easily recruited by low intensity stimuli than excitatory axons. This leads to a recruitment that favours inhibition, which results in an inhibitory dominated network response causing it to return a non-amplified network response.

Moreover, we explore how transient amplification can emerge from an excitation-inhibition imbalance, where the runaway excitation is eventually brought under control by inhibition. The amplification was shown by introducing statistical parameters that affect the initialization of our model.

In the depolarization case, we state that the direct electrical effect parameter $k$ captures the net effect of the field interacting with asymmetric axonal properties. We investigate a scenario where larger inhibitory axons are typically myelinated, which requires them to receive a higher intensity to activate, resulting in a bias in excitation recruitment. This suggests that myelination has a significant impact on the cortical response to stimulation.

Additionally, in the activation case, we explored the imbalance in the mean firing rate between excitation and inhibition to bring the network to a state of amplification. Similarly to the depolarization, the activation model relies on the antidromically activated axons and somas to activate the network. This suggests that excitatory axons and somas were readily recruited to amplify the network transiently.

Lastly, we briefly explored the unstable network response arising from unchecked runaway excitation. This results from a dominating excitatory input with no inhibition to slow the excitatory propagation.

Although these network responses were developed to describe cortical responses to external electrical stimulation, excitatory-inhibitory imbalances are not unique to electrical stimulation; they also occur in normal cortical function. Standard brain activity relies on balanced synaptic dynamics within local microcircuits, resulting in stable network responses. Unstable responses occur in a condition where there might be neurodegenerative microcircuitry that gives excitation the ability to remain unchecked. Transient amplification has been proposed to account for spontaneous activity patterns observed in the visual cortex. Thus, while the context is stimulation, these network responses do reflect a general organization of cortical function.

These findings suggest that a subtle difference in axonal properties can shift the network responses in our system during cortical stimulation. This can have significant implications for brain-computer interfaces, where specific stimulation patterns are required to treat certain neurodegenerative diseases.

## 5.2 Model Limitation

While the field model in this study offers a useful insight into the evoked network reactions from electrical stimulation and fine parameter tuning, we must acknowledge that, despite working within the realm of theory and assumptions, biology behaves differently.

The field model simplified the complexity of cortical circuits using a mean-field leaky integrate-and-fire framework, approximating synaptic dynamics with a population mean firing rate for both excitatory and inhibitory units. These simplifications limit the ability to capture the complex communications, such as synaptic plasticity, bursting, or history-dependent effects.

Additionally, the field model is a one-dimensional model with the assumption of homogeneous, isotropic tissue being stimulated, which loses the ability to understand behaviour in 2-3 dimensions with layer-specific connectivity. These additions likely influence the electrical spread of activation.

While the cable properties are grounded in physiological data for the intensity threshold relation with axon diameters, there are some additional functionalities that would make this thesis better.

In the derivation of the intensity threshold distribution (Equation 2.18), we used the conduction velocity for unmyelinated axons (Equation 2.11) to obtain our final results. Although we used unmyelinated assumptions, we truncated our distribution to account for myelinated inhibitory axons to benefit from excitatory recruitment. This results in a situation where large inhibitory axons are easily recruited through low intensity stimulation but large inhibitory axons are covered in a myelin sheath causing it to be less sensitive to low intensity stimulation. Therefore, exploring how myelination overcomes the effect of wide fibers would benefit in the exploration of this thesis.

In the results of axonal activation, we note that the larger inhibitory axons are part of the parvalbumin-positive cells giving us the ability to truncate our distribution and recruit more excitatory axons. However, due to the complexity of myelination patterns in excitatory neurons it becomes harder to set similar rules to influence the excitatory distribution [27, 26]. Investigating new functionalities to influence the intensity threshold distribution can give better and accurate results.

In the depolarization model, the direct electrical effect $k$ is related directly to the

effect caused by the electrical stimulation in our one-dimensional model. This variable alone does not directly show how the cable properties control transient amplification from electrical stimulation. The only link between the direct electrical effect and the cable properties is the recruitment ratio found in Figure 13**d**, which gives us the ratio we use for the direct electrical effect variable. However, the axonal recruitment ratio is not directly used to influence the direct electrical effect, but rather used as an approximation.

To bring it all together, while the models capture key dynamics and offer good insight, these limitations suggest that future work should incorporate more biologically detailed structures.

## 5.3 Future Work

Future work will focus on identifying the network parameters that optimize the excitatory signal propagation in the transient amplification response. In this study, we did not systematically examine how imbalances in synaptic connections affect signal propagation. Investigating how these parameters influence the spatial spread of activity could provide insight into how neurotherapeutic stimulation strategies might be optimized to target larger cortical regions and improve treatments for neurodegenerative disorders.

Additionally, the inhibitory/excitatory (I/E) imbalance ratio derived in our cable properties analysis was not explicitly incorporated in our depolarization model. Since electrical stimulation recruits more passing axons than individual somas, we obtain a sparse distribution of antidromically activated somas. A critical next step is to determine how this sparse distribution of activated neurons translates into the spatial distribution of voltage depolarization seen in Histed et al [14]. This eliminates the direct electrical effect parameter $k$ and finally utilizes the imbalance ratio from the recruited axons.

Finally, the current model assumes unmyelinated conduction velocity in deriving the intensity threshold distribution. Although the distribution was truncated to account for myelinated inhibitory axons to represent the subgroup of the larger inhibitory axons, future work should investigate how myelination alters the recruitment of wider fibers that are more sensitive to lower stimulation currents.

# 6 Conclusion

In this thesis, we investigated how differences in excitatory and inhibitory cable properties shape cortical responses to electrical stimulation. Through deriving analytical models and network simulations, we demonstrate that subtle biophysical differences, such as axon diameters and myelination, can significantly impact the network responses following stimulation.

We first derived the relationship between axon diameter and the intensity threshold from the cable theory and the strength-intensity curve. The cable theory introduces the framework and variables, such as the membrane time constant and the electronic constant. With this information, we were able to derive a relationship between conduction velocity, axon diameter, and chronoxie. Knowing that the axon diameter is normally distributed, we formally derive a new distribution for intensity threshold using variable changes. With the intensity threshold distribution, we found that large inhibitory axons are more likely to be recruited at lower stimulation intensities. This statistical asymmetry can bias the network response towards inhibition, suppressing excitatory propagation and leading to a non-amplified population response.

Later, based on the leaky integrate-and-fire definition, we constructed a mean-field approximation of the synaptic inputs from a network of excitatory and inhibitory cells distributed spatially in one dimension. Using this new derivation, we constructed two submodels, named the activation and depolarization models, that are initialized differently. The depolarization model utilizes the extracellular potential in conjunction with the direct electrical effect $k$. In comparison, the activation model utilizes synaptic rates from antidromic axonal and somatic activation to initiate the system, which is represented by the gain $\gamma$ and the likelihood of spatial spread following stimulation. Both models resulted in transient amplification, characterized by the initial runaway of excitation followed by inhibitory surpression. Additionally, we demonstrated cases where non-amplified and unstable conditions exist. These network responses only occur under specific parameter regimes, revealing a narrow window during which temporary excitation can dominate the network.

Our results demonstrate the importance of excitatory and inhibitory biophysical structures in determining different network responses following electrical stimulation. With these insights, there may be implications for brain-computer interfaces and therapeutic stimulation protocols, where targeting a specific cell group can help alleviate neurological disorders. Future work could explore a form of variable optimization for transient amplification that adheres to biological constraints and establishes the direct connection between the axonal activation ratio and the depolarization model.

# 7 Appendix

## 7.1 Definitions

The Dirac function $\delta(x)$:

$$\delta(x) = \begin{cases} \infty & \text{, if } \quad x = 0 \\ 0 & \text{, otherwise} \end{cases} \tag{7.1}$$

$$\int_{-\infty}^{\infty} \delta(x)dx = 1 \tag{7.2}$$

Convolution between two functions:

$$f(x) * g(x) = \int f(x-u)g(u)du \tag{7.3}$$

Heaviside definition:

$$\Theta(x) = \begin{cases} 1, & \text{if } \quad x \geq 0 \\ 0, & \text{if } \quad x < 0 \end{cases} \tag{7.4}$$

## 7.2 Analytical

All the code was written and compiled with Python 3.13 by Maxim Piatine.

Code can be found at:

https://github.com/MaxPiatine/microstim

### 7.2.1 Numerical Simulation

The connectivity is modelled with a Gaussian function of distance [11] characterized by a scale $\sigma$. The strength of the connection scales the Gaussian such that $\tilde{w}_{ee}(x) = \frac{W_{ee}}{\sigma\sqrt{2\pi}} \exp\left(\frac{-x^2}{2\sigma^2}\right)$, where $x$ is the distance between pre- and post-synaptic locations and $W_{ee}$ is the strength of the interaction.

The activation radii $\rho_e$ and $\rho_i$ are found by finding the threshold crossing point $V_T = V_e(\rho_e)$, and similarly for inhibition.

$$\tilde{w}_{ee}(x) = W_{ee} \cdot \mathcal{N}(x|\mu, \sigma_{ee}^2) = \frac{W_{ee}}{\sqrt{2\pi\sigma_{ee}^2}} e^{-\frac{1}{2}\frac{x^2}{\sigma_{ee}^2}} \tag{7.5}$$

$$\nu_e(x) = \Theta(V_e - V_T) = \begin{cases} 1 & \text{if } |x| \leq \rho_e, \\ 0 & \text{otherwise} \end{cases} \tag{7.6}$$

Now to convolve $w_{ee} * \nu_e$:

$$w_{ee} * \nu_e = \int W_{ee} \cdot \mathcal{N}(u|\mu, \sigma_{ee}^2)\nu(x-u)du = W_{ee} \int_{x-\rho_e}^{x+\rho_e} \frac{W_{ee}}{\sqrt{2\pi\sigma_{ee}^2}} e^{-\frac{1}{2}\frac{u^2}{\sigma_{ee}^2}} du \tag{7.7}$$

$$w_{ee} * \nu_e = \frac{W_{ee}}{2}\left[\text{erf}\left(\frac{x+\rho_e}{\sigma_{ee}}\right) - \text{erf}\left(\frac{x-\rho_e}{\sigma_{ee}}\right)\right] = \frac{W_{ee}}{2} K_{ee}(x;\rho_e) \tag{7.8}$$

where $K_{\alpha,\beta}|\alpha,\beta \in \{e,i\}$

$$K_{\alpha,\beta}(x;\rho_\alpha) = \text{erf}\left(\frac{x+\rho_\alpha}{\sigma_\alpha}\right) - \text{erf}\left(\frac{x-\rho_\alpha}{\sigma_\alpha}\right) \tag{7.9}$$

for the case of Gaussian connectivity and Heaviside functions.

The system dynamics that follow direct electrical stimulation is modeled after a first-order ordinary differential equation 3.17-3.18, where the model can be simulated efficiently by noting the forward-Euler formulation of the time-discretized potential $V_e^{(i)}$ reduces to

$$V_e^{(i)}(x) = V_e^{(i-1)}(x) + \Delta t \left[ -V_e^{(i-1)} + K_{ee}(x; \rho_e^{(i-1)}) - K_{ie}(x; \rho_i^{(i-1)}) \right] \tag{7.10}$$

$$V_i^{(i)}(x) = V_i^{(i-1)}(x) + \Delta t \left[ -V_e^{(i-1)} + K_{ei}(x; \rho_e^{(i-1)}) - K_{ii}(x; \rho_i^{(i-1)}) \right] \tag{7.11}$$

where the initial conditions are in Sections 4.2-4.3. In the depolarization model, the potential is driven by the direct electrical effect of intensity that recruited the ratio of excitatory and inhibitory axons. In the activation model, the initial condition to drive the potential into a propagation would depend on the mean rates.

For better accuracy, I've set the $\Delta t$ at one thousandth of a millisecond, while setting the spatial time step at a tenth of a micron. The rest of the parameters were dependent on the model and the type of propagation that come from the simulation.

# References


[1] World Health Organization. “Over 1 in 3 People Affected by Neurological Conditions: The Leading Cause of Illness and Disability Worldwide.” World Health Organization, 14 Mar. 2024, https://tinyurl.com/2dxxxkc3.

[2] Johnson, Kara A., et al. “Proceedings of the 11th Annual Deep Brain Stimulation Think Tank: Pushing the Forefront of Neuromodulation with Functional Network Mapping, Biomarkers for Adaptive DBS, Bioethical Dilemmas, AI-Guided Neuromodulation, and Translational Advancements.” Frontiers in Human Neuroscience, vol. 18, 2024, article no. 1320806, https://doi.org/10.3389/fnhum.2024.1320806.

[3] Dahodwala, Nabila, et al. “Prevalence and Correlates of Anti-Parkinson Drug Use in a Nationally Representative Sample.” Movement Disorders Clinical Practice, vol. 4, no. 3, 2016, pp. 335–341. https://doi.org/10.1002/mdc3.12422.

[4] Parkinson’s UK. “Parkinson’s Medication Fails to Control Symptoms for Nearly 75% of People.” Parkinson’s UK, 14 Mar. 2024, https://tinyurl.com/4au7br7s.

[5] professional, C. C. medical. (2025, March 19). Deep Brain Stimulation (DBS): What it is, Purpose & procedure. Cleveland Clinic. https://my.clevelandclinic.org/health/treatments/21088-deep-brain-stimulation

[6] Cleveland Clinic. “Basal Ganglia.” Cleveland Clinic, 13 July 2023, https://my.clevelandclinic.org/health/body/23962-basal-ganglia. Accessed 22 July 2025.

[7] Hitti, Frederick L., et al. “Long-Term Outcomes Following Deep Brain Stimulation for Parkinson’s Disease.” Journal of Neurosurgery, vol. 132, no. 1, 2019, pp. 205–210. https://doi.org/10.3171/2018.8.JNS182081.

[8] Gerstner, W., Kistler, W. M., Naud, R., & Paninski, L. (2016). Neuronal dynamics from single neurons to networks and models of cognition Wulfram Gerstner; Werner M. Kistler; Richard Naud; Liam Paninski. Cambridge University Press.

[9] Nowak, L. G., and J. Bullier. “Axons, but Not Cell Bodies, Are Activated by Electrical Stimulation in Cortical Gray Matter. I. Evidence from Chronaxie Measurements.” Experimental Brain Research, vol. 118, no. 4, Feb. 1998, pp. 477–488. https://doi.org/10.1007/s002210050304.

[10] Micheva, Kristina D., et al. “A Large Fraction of Neocortical Myelin Ensheathes Axons of Local Inhibitory Neurons.” eLife, vol. 5, 6 July 2016, e15784. https://doi.org/10.7554/eLife.15784.

[11] Campagnola, Luke, et al. “Local Connectivity and Synaptic Dynamics in Mouse and Human Neocortex.” Science, vol. 375, no. 6581, 2022, eabj5861. https://doi.org/10.1126/science.abj5861.

[12] Stoney, S. D., Thompson, W. D., & Asanuma, H. (1968). Excitation of pyramidal tract cells by intracortical microstimulation: Effective extent of stimulating current. Journal of Neurophysiology, 31(5), 659–669. https://doi.org/10.1152/jn.1968.31.5.659

[13] Kumaravelu, Karthik, et al. “Stoney vs. Histed: Quantifying the Spatial Effects of Intracortical Microstimulation.” Brain Stimulation, vol. 15, no. 1, 2022, pp. 141–151. https://doi.org/10.1016/j.brs.2021.11.015.

[14] Histed, Mark H., Vincent Bonin, and Karel Svoboda. “Direct Activation of Sparse, Distributed Populations of Cortical Neurons by Electrical Microstimulation.” Neuron, vol. 63, no. 4, 2009, pp. 508–522. https://doi.org/10.1016/j.neuron.2009.07.016.

[15] Koch, C. Cable theory in neurons with active, linearized membranes. Biol. Cybern. 50, 15–33 (1984). https://doi.org/10.1007/BF00317936

[16] Benson, Alan P., et al. ”Multi-Scale Approaches for the Simulation of Cardiac Electrophysiology: II – Tissue-Level Structure and Function.” Methods, vol. 185, 2021, pp. 60–81. ScienceDirect, https://doi.org/10.1016/j.ymeth.2020.01.010.

[17] Rattay, Frank. “Analysis of Models for External Stimulation of Axons.” IEEE Transactions on Bio-Medical Engineering, vol. 33, no. 10, 1986, pp. 974–977. https://doi.org/10.1109/TBME.1986.325670.

[18] Swadlow, Harvey A. “Monitoring the Excitability of Neocortical Efferent Neurons to Direct Activation by Extracellular Current Pulses.” Journal of Neurophysiology, vol. 68, no. 2, 1992, pp. 605–619. https://doi.org/10.1152/jn.1992.68.2.605.

[19] West, D. C., and J. H. Wolstencroft. “Strength-Duration Characteristics of Myelinated and Non-Myelinated Bulbospinal Axons in the Cat Spinal Cord.” The Journal of Physiology, vol. 337, 1983, pp. 37–50. https://doi.org/10.1113/jphysiol.1983.sp014610.

[20] Brunel, Nicolas, and Mark C. W. van Rossum. “Lapicque’s 1907 Paper: From Frogs to Integrate-and-Fire.” Biological Cybernetics, vol. 97, no. 5-6, 2007, pp. 337–339. https://doi.org/10.1007/s00422-007-0190-0.

[21] Gerstner, Wulfram, and Werner M. Kistler. Spiking Neuron Models, 15 Aug. 2002, https://doi.org/10.1017/cbo9780511815706.

[22] Rosenbaum, Robert, and Brent Doiron. ”Balanced Networks of Spiking Neurons with Spatially Dependent Recurrent Connections.” Phys. Rev. X, vol. 4, no. 2, May 2014, article 021039, 9 pages. American Physical Society, https://doi.org/10.1103/PhysRevX.4.021039.

[23] Radman, Thomas, et al. “Role of Cortical Cell Type and Morphology in Subthreshold and Suprathreshold Uniform Electric Field Stimulation In Vitro.” Brain Stimulation, vol. 2, no. 4, 2009, pp. 215–228.e3. https://doi.org/10.1016/j.brs.2009.03.007.

[24] Shapson-Coe, Alexander, et al. “A Petavoxel Fragment of Human Cerebral Cortex Reconstructed at Nanoscale Resolution.” Science, vol. 384, no. 6696, 2024, eadk4858. https://doi.org/10.1126/science.adk4858.

[25] Braun, Jochen. Lecture 7: Modeling Morphology. Theoretical Neuroscience I, Otto-von-Guericke-Universität Magdeburg, Cognitive Biology Group, Winter 2018/19. https://tinyurl.com/w98avum8.

[26] Micheva, Kristina D., et al. “Distinctive Structural and Molecular Features of Myelinated Inhibitory Axons in Human Neocortex.” eNeuro, vol. 5, no. 5, 16 Oct. 2018, ENEURO.0297-18.2018. https://doi.org/10.1523/ENEURO.0297-18.2018.

[27] Stedehouder, Jeffrey, et al. “Local Axonal Morphology Guides the Topography of Interneuron Myelination in Mouse and Human Neocortex.” eLife, vol. 8, 19 Nov. 2019, e48615. https://doi.org/10.7554/eLife.48615.

[28] Tomassy, Giulio Srubek, et al. “Distinct Profiles of Myelin Distribution along Single Axons of Pyramidal Neurons in the Neocortex.” Science, vol. 344, no. 6181, 2014, pp. 319–324. https://doi.org/10.1126/science.1249766.

[29] Nelson, Philip Charles, et al. Biological Physics: Energy, Information, Life. W.H. Freeman and Co., 2004.

[30] Giuliodori, Mauricio J., and Stephen E. DiCarlo. ”Myelinated vs. Unmyelinated Nerve Conduction: A Novel Way of Understanding the Mechanisms.” Advances in Physiology Education, vol. 28, no. 2, 2004, pp. 80–81. American Physiological Society, https://doi.org/10.1152/advan.00045.2003.

[31] Susuki, Keiichiro. ”Myelin: A Specialized Membrane for Cell Communication.” Nature Education, vol. 3, no. 9, 2010, p. 59.

[32] Goldman, L., and J. S. Albus. “Computation of Impulse Conduction in Myelinated Fibers; Theoretical Basis of the Velocity-Diameter Relation.” Biophysical Journal, vol. 8, no. 5, 1968, pp. 596–607. https://doi.org/10.1016/S0006-3495(68)86510-5.

[33] Hursh, J. B. ”The Properties of Growing Nerve Fibers.” American Journal of Physiology, vol. 127, no. 1, 1939, pp. 140–153. https://doi.org/10.1152/ajplegacy.1939.127.1.140.

[34] McNeal, D. R. “Analysis of a Model for Excitation of Myelinated Nerve.” IEEE Transactions on Bio-Medical Engineering, vol. 23, no. 4, 1976, pp. 329–337. https://doi.org/10.1109/tbme.1976.324593.

[35] Okun, Michael, and Ilan Lampl. ”Balanced Cortical Activity.” Scholarpedia, vol. 4, no. 8, 2009, p. 7467, https://doi.org/10.4249/scholarpedia.7467.

[36] Caire, Michael J., Vikas Reddy, and Mark A. Varacallo. ”Physiology, Synapse.” StatPearls, updated 27 Mar. 2023, StatPearls Publishing, 2025, https://www.ncbi.nlm.nih.gov/books/NBK526047/.

[37] ”What Defines a Neurotransmitter?” Neuroscience, edited by Dale Purves, George J. Augustine, David Fitzpatrick, et al., 2nd ed., Sinauer Associates, 2001, https://www.ncbi.nlm.nih.gov/books/NBK10957/.

[38] ”Electrical Synapses.” Neuroscience, edited by Dale Purves, George J. Augustine, David Fitzpatrick, et al., 2nd ed., Sinauer Associates, 2001, https://www.ncbi.nlm.nih.gov/books/NBK11164/.

[39] Brain Basics: The Life and Death of a Neuron — National Institute of Neurological Disorders and Stroke, https://tinyurl.com/5d3y9mtb. Accessed 15 July 2025.

[40] Chrysafides, Steven M., Samuel J. Bordes, and Sandeep Sharma. "Physiology, Resting Potential." StatPearls, updated 10 Apr. 2023, StatPearls Publishing, 2025, https://www.ncbi.nlm.nih.gov/books/NBK538338/.

[41] Grider, Michael H., Rahul Jessu, and Rifat Kabir. "Physiology, Action Potential." StatPearls, updated 8 May 2023, StatPearls Publishing, 2025, https://www.ncbi.nlm.nih.gov/books/NBK538143/.

[42] Biga, Lindsay M., et al. "12.5 the Action Potential." Anatomy & Physiology, OpenStax/Oregon State University, 26 Sept. 2019, open.oregonstate.education/aandp/chapter/12-5-the-action-potential/.

[43] Zhang, Hongyu, et al. "Brain-Computer Interfaces: The Innovative Key to Unlocking Neurological Conditions." International Journal of Surgery (London, England), vol. 110, no. 9, 1 Sept. 2024, pp. 5745–5762. https://doi.org/10.1097/JS9.0000000000002022.

[44] Anastassiou, Costas A., Roxanne Perin, Henry Markram, and Christof Koch. "Ephaptic Coupling of Cortical Neurons." Nature Neuroscience, vol. 14, no. 2, 2011, pp. 217–223, https://doi.org/10.1038/nn.2727.

[45] Geddes, L. A., and J. D. Bourland. "The Strength-Duration Curve." IEEE Transactions on Biomedical Engineering, vol. BME-32, no. 6, 1985, pp. 458–459, https://doi.org/10.1109/TBME.1985.325456.

[46] Gilbert, Zachary, et al. "A Review of Neurophysiological Effects and Efficiency of Waveform Parameters in Deep Brain Stimulation." Clinical Neurophysiology, vol. 152, 2023, pp. 93–111, https://doi.org/10.1016/j.clinph.2023.04.007.

[47] Trebaul, Lena, et al. "Stimulation Artifact Correction Method for Estimation of Early Cortico-Cortical Evoked Potentials." Journal of Neuroscience Methods, vol. 264, 2016, pp. 94–102. https://doi.org/10.1016/j.jneumeth.2016.03.002.

[48] Trebaul, Lena, et al. "Probabilistic Functional Tractography of the Human Cortex Revisited." NeuroImage, vol. 181, 2018, pp. 414–429. https://doi.org/10.1016/j.neuroimage.2018.07.039.

[49] Mayberg, Helen S., et al. "Deep Brain Stimulation for Treatment-Resistant Depression." Neuron, vol. 45, no. 5, 2005, pp. 651–660. https://doi.org/10.1016/j.neuron.2005.02.014.

[50] Laxton, Adrian W., et al. "Deep Brain Stimulation for Cognitive Disorders." Handbook of Clinical Neurology, vol. 116, 2013, pp. 307–311. https://doi.org/10.1016/B978-0-444-53497-2.00025-5.

[51] Mankin, Emily A., and Itzhak Fried. "Modulation of Human Memory by Deep Brain Stimulation of the Entorhinal-Hippocampal Circuitry." Neuron, vol. 106, no. 2, 2020, pp. 218–235. https://doi.org/10.1016/j.neuron.2020.02.024.

[52] Skarpaas, Tara L., et al. "Brain-Responsive Neurostimulation for Epilepsy (RNS® System)." Epilepsy Research, vol. 153, 2019, pp. 68–70. https://doi.org/10.1016/j.eplepsyres.2019.02.003.

[53] Morgante, Letterio, et al. “How Many Parkinsonian Patients Are Suitable Candidates for Deep Brain Stimulation of Subthalamic Nucleus? Results of a Questionnaire.” Parkinsonism & Related Disorders, vol. 13, no. 8, 2007, pp. 528–531. https://doi.org/10.1016/j.parkreldis.2006.12.013.

[54] Bishay, Anthony E., et al. “Global Economic Evaluation of the Reported Costs of Deep Brain Stimulation.” Stereotactic and Functional Neurosurgery, vol. 102, no. 4, 2024, pp. 257–274. https://doi.org/10.1159/000537865.

[55] Rasiah, Neilen P., et al. ”Complications of Deep Brain Stimulation for Parkinson Disease and Relationship between Micro-Electrode Tracks and Hemorrhage: Systematic Review and Meta-Analysis.” World Neurosurgery, vol. 171, 2023, pp. e8–e23, https://doi.org/10.1016/j.wneu.2022.10.034.

[56] Rao, Vikram R., and Daniel H. Lowenstein. ”Epilepsy.” Current Biology, vol. 25, no. 17, 2015, pp. R742–R746, https://doi.org/10.1016/j.cub.2015.07.072.

[57] Hennequin, Guillaume, Tim P. Vogels, and Wulfram Gerstner. ”Non-normal amplification in random balanced neuronal networks.” Physical Review E, vol. 86, no. 1, pt. 1, 2012, p. 011909. https://doi.org/10.1103/PhysRevE.86.011909.

[58] Kenet, Tal, Dmitri Bibitchkov, Misha Tsodyks, Amiram Grinvald, and Amiram Arieli. ”Spontaneously Emerging Cortical Representations of Visual Attributes.” Nature, vol. 425, no. 6961, 2003, pp. 954–956. https://doi.org/10.1038/nature02078.

[59] Wilson, H.R., Cowan, J.D. A mathematical theory of the functional dynamics of cortical and thalamic nervous tissue. Kybernetik 13, 55–80 (1973). https://doi.org/10.1007/BF00288786

[60] Markounikau, Valentin, et al. “A Dynamic Neural Field Model of Mesoscopic Cortical Activity Captured with Voltage-Sensitive Dye Imaging.” PLoS Computational Biology, vol. 6, no. 9, 2010, e1000919. Public Library of Science, https://doi.org/10.1371/journal.pcbi.1000919.

[61] Wen, Q., and Dmitri B. Chklovskii. “To Myelinate or Not to Myelinate?” New Aspects of Axonal Structure and Function, edited by Dirk Feldmeyer and Joachim Lübke, Springer, 2010, pp. 135–161. SpringerLink, https://doi.org/10.1007/978-1-4419-1676-1_6